Characterization of Zebrafish Mutants to Model Human Genetic Defects in the *LRRC56* gene.

Joshua Ivare

Thesis submitted to the University of Ottawa in partial fulfilment of the requirements for the Master of Science in Biology Program

Department of Biology

Faculty of Science

University of Ottawa

Abstract

In humans, defects of motile cilia are characterized by respiratory infections, in some cases, congenital heart disease, and in about 50% of patients, laterality defects where the proper placement of internal organs is disrupted. Recently, two autopsied human fetuses identified as carrying a homozygous missense variant of the Leucine-rich repeat (LRR)-containing gene 56 (*LRRC56*) gene showed mirror image placement of thoracic and abdominal structures as well as complex cardiac anomalies. Furthermore, *LRRC56* was recently reported to be a homolog of the Outer Dynein Arm 8 gene (*oda8*), a gene necessary for the cytoplasmic maturation of the outer dynein arms (ODA) in the flagella of algae. Therefore, to confirm that the observed phenotypes of the human fetuses are the result of an inactive LRRC56 protein, we created a zebrafish *lrrc56* knockout with a 4bp deletion in the first exon of the *lrrc56* gene (*lrrc56*$^{-/-}$) using the CRISPR/Cas9 genome editing technology. We hypothesize that if the missense mutation of the *LRRC56* gene in the human fetuses indeed renders the LRRC56 protein inactive, a knockout of the zebrafish *lrrc56* gene might produce in zebrafish similar phenotypes to those observed in the mutant human fetuses. We show that knocking out the zebrafish *lrrc56* gene leads to spinal defects in the *lrrc56*$^{-/-}$ zebrafish. By performing gene expression analyses on the *lrrc56*$^{-/-}$ mutants, we observed defects in visceral organ left/right asymmetry. Injection of the wild type *lrrc56* mRNA rescued the phenotypes of spinal and visceral organ asymmetry defects in the *lrrc56*$^{-/-}$ mutants while the injection of a *lrrc56* mRNA possessing the same missense mutation observed in the two autopsied fetuses failed to rescue these phenotypes. When we performed IHC with an α-tubulin antibody to detect cilia in the zebrafish Kupffer's Vesicle (KV), we observed that the cilia present in the KV of the *lrrc56*$^{-/-}$ mutants were longer than those in WT zebrafish. Together, our results verify that

the observed phenotypes of the fetuses are due to the homozygous missense *LRRC56* variant they possessed.

Acknowledgements

I would like to thank my supervisor Dr. Marie-Andrée Akimenko for giving me the opportunity to pursue research for my master's project in her laboratory. I learnt a lot about science and research work under her tutelage. Even when results did not exactly go my way, her constant focus, guidance and dynamic thinking allowed me to maintain my own focus and in turn improve my critical thinking and troubleshooting abilities.

Furthermore, I would like to thank my committee members, Dr. Marc Ekker and Dr. Bruce McKay for making comments and asking the questions that helped keep my project on course.

Special thanks to Dr. Marc Ekker for graciously allowing me to work on parts of my project in his lab.

I would also like to thank Vishal Saxena, my friend and mentor for his guidance and mentorship throughout this project. His sense of humor, knowledge and his brilliant troubleshooting abilities made working with him daily a pleasure. From the hours spent in the fish-room to the time spent in the lab, working with him was never boring.

I would like to also thank our previous lab technician Jing Zhang for always being present, patient and very willing to answer my questions even when I was asking almost 20 questions a day. I really do not think I would have made it through this project without her unwavering support.

I would also like to thank members of the Akimenko Lab for providing a great work atmosphere and the most interesting conversation topics.

Finally, I also want to thank our collaborator at CHEO, Dr. Kym Boycott, all the members of the Ekker lab, the Animal Control and veterinary Services (ACVS) team at uOttawa, and the University of Ottawa Department of Biology.

Table of Contents

List of Figures

List of Abbreviations

aa	amino acid
CHEO	Children's Hospital of Eastern Ontario
BCIP	5-Bromo-4-chloro-3-indolyl phosphate
bp	base pair(s)
cAMP	cyclic adenosine monophosphate
Cas	CRISPR associated -
cDNA	complementary DNA
CDS	Coding Sequence
cmlc1	*cardiac myosin light chain type 1*
crRNA	CRISPR RNA
CRISPR	Clustered Regularly Interspaced Short Palindromic **r**epeats
DFCs	Dorsal Forerunner Cells
Dpf	days post fertilization
DRC	Dynein Regulatory Complex
DSB	Double Strand Break
DAPI	4,6-diamidino-2-phenylindole
DIG	Digoxygenin
EDTA	Ethylenediaminetetraacetic acid
F_0	Primary Injected Generation
F_1	First Filial Generation
foxA3	*forkhead box A3*
GFP	Green Fluorescent Protein
HFA	Heteroduplex Formation Assay
HDR	Homology Directed Repair
Hpf	hours post fertilization
IDA	Inner Dynein Arm
IFT	Intraflagellar Transport
IHC	Immunohistochemistry

ISH	*in situ* hybridization
KOH	Potassium Hydroxide
KV	Kupffer's Vesicle
L/R	left-right
lefty1	*left-right determination factor 1*
LPM	Lateral Plate Mesoderm
LRO	Left-Right Organizer
lrrc56$^{-/-}$	*lrrc56* mutants homozygous for the *lrrc56*^{ot113} allele
lrrc56^{ot113}	*lrrc56* allele with a 4bp deletion in the 1st exon
lrrc56^{ot114}	*lrrc56* allele with a 4bp insertion in the 1st exon
LRRC-	*Leucine Rich Repeat Containing Gene* –
MAPK	mitogen-activated protein kinase
mRNA	messenger RNA
NBT	Nitro Blue Tetrazolium
NHEJ	Non-Homologous End Joining
ODA	Outer Dynein Arm
ODA-AC	Outer Dynein Arm Assembly Complex (*oda5/10)*
ODA-DC	Outer Dynein Arm Docking Complex
p.Leu140Pro	Leucine to Proline substitution at the 140th aa position
PA	Poly-A sequence
PAGE	Poly-Acrylamide Gel Electrophoresis
PBS	Phosphate Buffered Saline
PBST	Phosphate Buffered Saline with Tween 20
PCD	Primary Ciliary Dyskinesia
PCR	Polymerase Chain Reaction
PP-1	protein phosphatase-1
PTU	1-phenyl 2-thiourea
RT-PCR	Reverse Transcriptase Polymerase Chain Reaction
SDM	Site Directed Mutagenesis
sgRNA	synthetic single guide RNA

SNP	Single Nucleotide Polymorphism
TBE	Tris/Borate/EDTA
Tg	Transgenic line
trRNA	trans-activating crRNA
UTR	Untranslated Region
WT	Wild Type
ZFIN	Zebrafish Information Network

1.0 Introduction

1.1 Background Information

Pathologists at the Children's Hospital of Eastern Ontario (CHEO) recently identified 2 related stillborn fetuses with asymmetry defects (*situs inversus*) of thoracic and abdominal structures as well as complex cardiac anomalies, suggestive of a cilia-related disease. Subsequent whole exome sequencing of tissues from one fetus by Dr. Kym Boycott's group identified twelve rare homozygous gene variants. Through a database and literature search, of these twelve genes, the *LRRC56* gene was singled out as the only gene with a role in the assembly of cilia due to the presence of an algal ortholog with a similar function in ciliary formation. The second fetus was also discovered to possess this same homozygous variant of the *LRRC56* gene.

1.2 Basic Structure and Function of Motile Cilia

Cilia and flagella are structurally similar microtubular organelles differing only in their length, number per cell and type of movement (Christensen, Pedersen, Schneider, & Satir, 2006; Pan, 2008) that project from the surface of cells in many eukaryotic organisms. Originally, the term "cilia" was used to describe a large number of relatively short structures such as seen in *Paramecium* while the term "flagellum" was applied to a single long structure in cells such as sperm (Murray, Larson, Masyuk, Masyuk, & LaRusso, 2010). In humans, there are two subtypes of cilia that can be found in the body: motile and non-motile cilia (Murray, Larson, Masyuk, Masyuk, & LaRusso, 2010). A non-motile cilium is a single cilium that arises when the centriole inherited during a previous mitotic cell division pushes out an extension of the plasma membrane supported by doublet microtubules which are continuous with the triplet microtubules of the centriole. Therefore, non-motile cilia project from the surface of every cell (Sorokin, 1962; Sorokin, 1968). On the other hand, motile cilia exist and project in large numbers from the epithelial surfaces of the respiratory tract, middle ear, the ventricles of the central nervous system, and the fallopian tubes (Valente, & Mitchison, 2016). Both motile and non-motile cilia act as antennae for sensing extracellular signals which include growth factors, fluid flow, developmental morphogens and noxious compounds (Berbari, O'Connor, Haycraft, & Yoder, 2009; Goetz & Anderson, 2010; Louvi & Grove, 2011; Veland, Awan, Pedersen, Yoder, & Christensen, 2009; Shah et al., 2009). To sense extracellular signals, a wide spectrum of signaling receptors are concentrated in the ciliary compartment, separated from the rest of the cell by diffusional barriers at the base of the cilia or on the cilia themselves (Nachury, Seeley, & Jin, 2010, Shah et al., 2009). Furthermore, both types of cilia exert mechanical force. On one hand, non-motile cilia exert mechanical force by bending to initiate signaling cascades (Praetorius & Spring, 2001; Nauli et

al., 2008), while on the other hand, motile cilia exert mechanical force through their rotational movement to generate extracellular fluid flow (Sawamoto, 2006; Yoshiba & Hamada, 2014). Due to their ability to generate extracellular fluid flow, we will be focusing on motile cilia.

Structurally, motile cilia possess a central bundle of microtubule doublets, comprised of a complete microtubule with 13 tubulin dimer protofilaments (A-tubule) and an incomplete microtubule of 10 tubulin protofilaments (B-tubule) (Fig. 1), called the axoneme that can be arranged in different conformations. Based on these arrangements of the axoneme, two types of motile cilia were identified in humans: motile cilia with the axoneme arranged in a '9 + 2' formation (Fig. 1), and motile cilia with the axoneme arranged in a '9 + 0' formation (Fliegauf et al., 2007). Motile cilia with the '9 + 0' axoneme formation lack the central pair of singlet microtubules seen in the '9 + 2' formation (Fig. 1). Each outer microtubule doublet is linked to the adjacent microtubule doublets by a protein called nexin (Fig. 1). Furthermore, the radial spokes act as spacers to position each outer doublet in a circle around the central pair of singlet microtubules (Fig. 1, Lindemann & Lesich, 2010). The radial spokes are then anchored to each outer doublet near the Dynein Regulatory Complex (DRC). Both the radial spokes and the DRC have previously been shown to contain calcium-binding proteins (centrin in the DRC and calmodulin in the spokes) evidenced by all cilia responding to free calcium by altering their beating pattern (Lindemann & Lesich, 2010).

Though motile cilia generally function by moving extracellular fluid, their specific functions depend on their locations. For example, in the respiratory tract, motile cilia produced by the respiratory epithelial cells in conjunction with mucus-producing epithelial goblet cells form a mucociliary escalator that moves mucus containing trapped pathogens, debris and pollutants up or down the throat to be expelled or ingested (Valente, & Mitchison, 2016; Mall, 2008; Wanner, Salathé, & O'Riordan, 1996). In the central nervous system, cilia from the ependymal cells that

line the ventricles of the brain and the central canal of the spinal cord, create cerebrospinal fluid flow which is responsible for moving signalling molecules through the central nervous system (Ibañez-Tallon et al., 2004, Faubel, Westendorf, Bodenschatz, & Eichele, 2016).

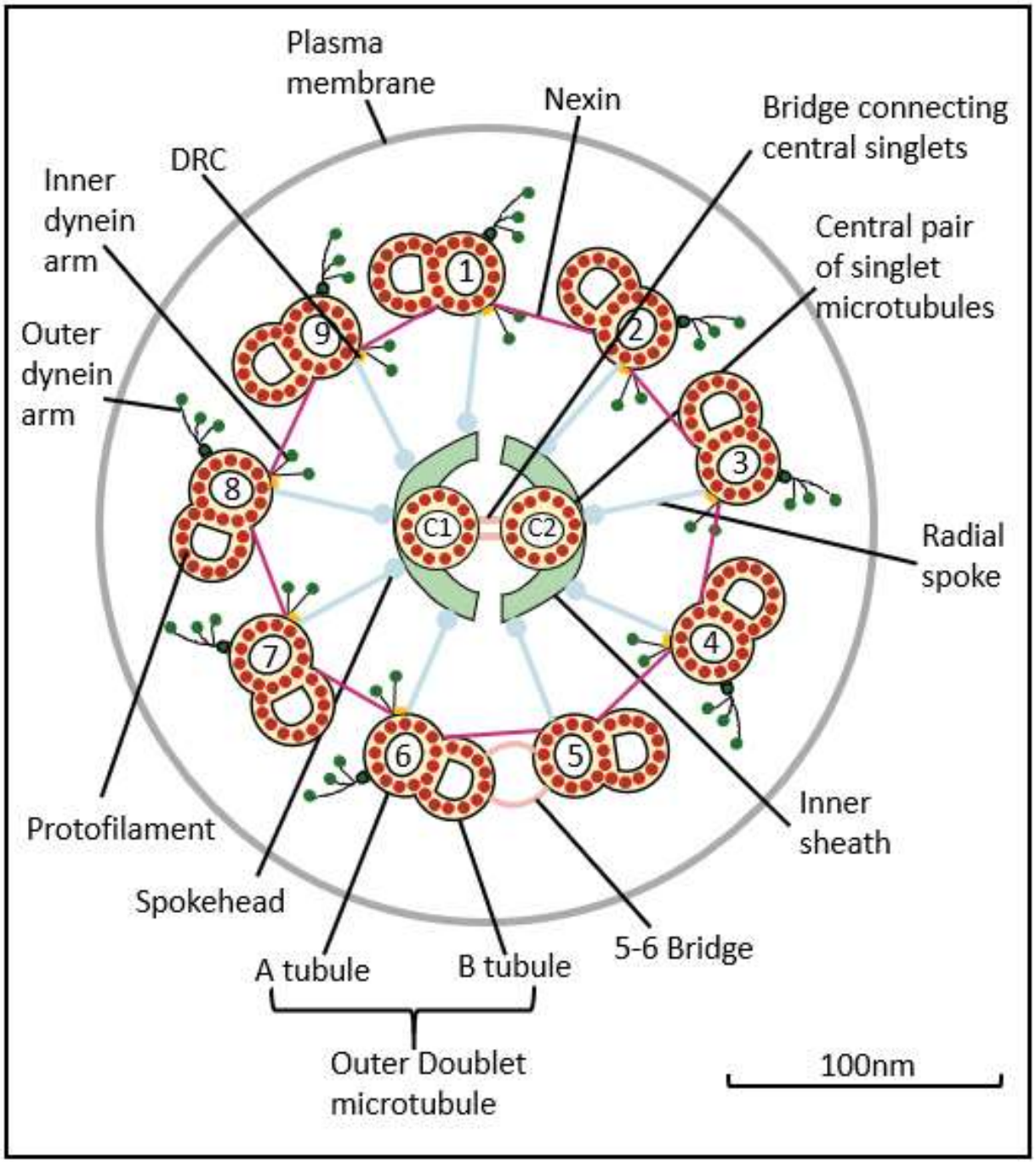

Fig. 1. Cross-section of a '9 + 2' motile cilium showing its major structures. Within the axoneme, there are two central singlet microtubules and nine outer doublet microtubules that are continuous for the entire length of the cilium. The outer and inner dynein arms are permanently attached to the A tubule of doublets 1-4, 6-9. DRC, Dynein Regulatory Complex

1.3 Defects of Axonemal Dyneins are associated with Ciliopathies.

Dyneins are one of the three families of ATPase cytoskeletal motor proteins in cells (Roberts, Kon, Knight, Sutoh, & Burgess, 2013). They provide the driving force for cilia motility and contribute to microtubule-based cargo transport within cells (Pfister, 2015; Porter, 1996). Dyneins are built around force-generating subunits called heavy chains, so termed because of their large molecular mass ~500 kilodaltons (Burgess, Walker, Sakakibara, Knight, & Oiwa, 2003; Roberts, Kon, Knight, Sutoh, & Burgess, 2013). Phylogenetically, based on their heavy chains, dyneins are grouped into nine major classes (Wickstead & Gull, 2007). Seven of these nine major dynein classes are built into the axoneme, where they power ciliary beating (Roberts, Kon, Knight, Sutoh, & Burgess, 2013). Cytoplasmic dyneins which are responsible for transporting cytoplasmic cargos containing cytoskeletal filaments like intermediate filaments and microtubules, viruses, protein complexes like mitotic-check point proteins, membrane-bound organelles like endosomes, lysosomes, mitochondria and nuclei, make up one of the two remaining classes. The intraflagellar transport dyneins, found exclusively in the ciliary compartment, which are involved in the retrograde movement [intraflagellar transport (IFT)] of multi-subunit protein complexes, called IFT particles, along axonemal microtubules beneath the ciliary membrane (Hao & Scholey, 2009) (Fig. 2) are the last major class of dyneins (Roberts, Kon, Knight, Sutoh, & Burgess, 2013; Pigino et al., 2009).

In cilia, the axonemal dyneins are further subdivided into inner and outer arms, depending on their position (Gibbons, 1963). Each outer dynein arm (ODAs) consists of three different dynein heavy chains while the inner dynein arms (IDAs) comprise eight different dynein heavy chains (Roberts, Kon, Knight, Sutoh, & Burgess, 2013). Currently, the best insight to the arrangement of these dynein arms are from the green algae *Chlamydomonas reinhardtii*, through molecular, genetic and

cryo-electron tomography studies (Fig. 3, Nicastro, 2009). In motile cilia, axonemal dyneins that form the inner and outer dynein arms are attached to the A tubule of the outer doublets with the inner dynein arms in close contact with the DRC (Fig. 1); These dynein arms on the A tubule of one outer doublet then interact transiently with the B tubule of the adjacent outer microtubule doublet to produce inter-doublet sliding and ciliary motion (Porter, 1996). Furthermore, the dynein arms on one side of the axoneme bend the cilium in one direction of a beating cycle (Fig. 2) while the dynein arms on the opposite side of the axoneme contribute to bending the cilium in the opposite direction. In motile cilia, doublets 5 and 6 are permanently linked to each other and cannot slide relative to each other (Afzelius, 1959). Doublet 1, which is located approximately 90 degrees to the central pair of singlet microtubules (Fig. 1), and doublets 2-4 are the first group whose dynein arms bend the axoneme in one direction during cilia beating. Doublets 6-9 bend the axoneme in the opposite direction (Lindemann & Lesich, 2010).

Motile cilia, beat in an asymmetric whip-like motion (Dutcher, 1995). This whip-like motion also known as a waveform has previously been shown through experiments with *Chlamydomonas reinhardtii* to be established and maintained by the axonemal IDAs (Dutcher, 1995; Van Rooijen et al., 2008). Further experiments with *Chlamydomonas reinhardtii* demonstrated that while ODAs are not involved in establishing cilia waveform, they influence the ciliary beat velocity as ODA *Chlamydomonas reinhardtii* mutants demonstrated about a third of the cilia beat velocity compared to WT (Kamiya, 1988; Dutcher, 1995). As mentioned previously, through their whip-like motion, motile cilia generate extracellular fluid flow and the function of this flow is highly dependent on its location. In addition to the examples mentioned previously in the brain and respiratory tract, extracellular fluid flow generated by motile cilia in an organ known as the "Left-Right Organizer" (LRO) during early development determines the sinistrality or dextrality of

asymmetrically located visceral organs in otherwise bilaterally-symmetric vertebrates (Desgrange, Le Garrec, & Meilhac, 2018).

Furthermore, genetic defects leading to the malformation of structural components of motile cilia including axonemal dyneins (Fig. 4) and the resulting interference in motile ciliary motion have previously been shown to cause defects that are collectively known as ciliopathies which can be sometimes lethal (Guichard et al., 2001; Reiter & Leroux, 2017). These ciliopathies include defects such as *situs inversus* and a disease known as known as Primary Ciliary Dyskinesia (PCD) in many animals (Guichard et al., 2001). *situs inversus* is a genetic condition that is found in approximately 0.01% of the human population (Jain, Jain, & Gupta, 2011). It occurs when the major asymmetrically located visceral organs like the heart, stomach, liver and spleen are transposed from their normal positions to the opposite side of the body (Fig. 5) and it exists in two forms. With an incidence of 1:8,000 newborn births (Mujo, Finnegan, Joshi, Wilcoxen, & Reed, 2015), *situs inversus totalis* occurs when there is a complete reversal of visceral organ position. In contrast, with an incidence of 1:10,000 newborn births (Mujo, Finnegan, Joshi, Wilcoxen, & Reed, 2015), *situs ambiguus* (heterotaxy) occurs when the visceral organ position reversals are random (Pennekamp et al., 2015). Unlike s*itus inversus totalis* which is often undiscovered in human patients until adulthood due to almost no apparent physiologic consequences, heterotaxy is accompanied by congenital heart disease in 50% -100% of identified cases (Applegate, Goske, Pierce, & Murphy, 1999). In fact, patients with heterotaxy account for approximately 4% of all identified congenital heart defect cases (Paladini & Volpe, 2007). On the other hand, PCD is a syndrome that is associated with *situs* abnormalities, abnormal sperm motility, and abnormal ciliary structure and function that result in retention of mucus and bacteria in the respiratory tract (Knowles, Zariwala, & Leigh, 2016). In humans, PCD results in chronic airway infections and

chronic/recurrent ear infections which both persist till adulthood. Furthermore, *Situs inversus totalis* is also present in 40%-50% of individuals with PCD while heterotaxy is present in at least 12% (Knowles, Zariwala, & Leigh, 2016).

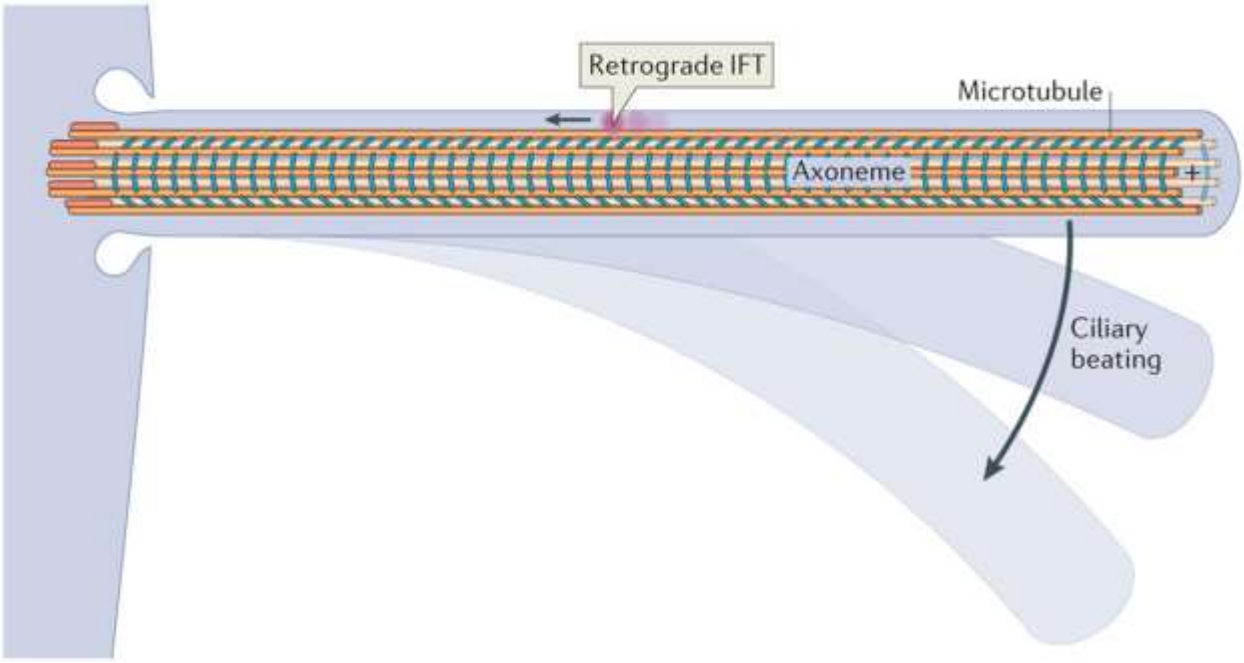

Fig. 2 Dynein functions in cilia. Intraflagellar transport (IFT) dynein (pink) performs retrograde IFT, whereas axonemal dyneins (cyan) power the beating of motile cilia (Roberts, Kon, Knight, Sutoh, & Burgess, 2013).

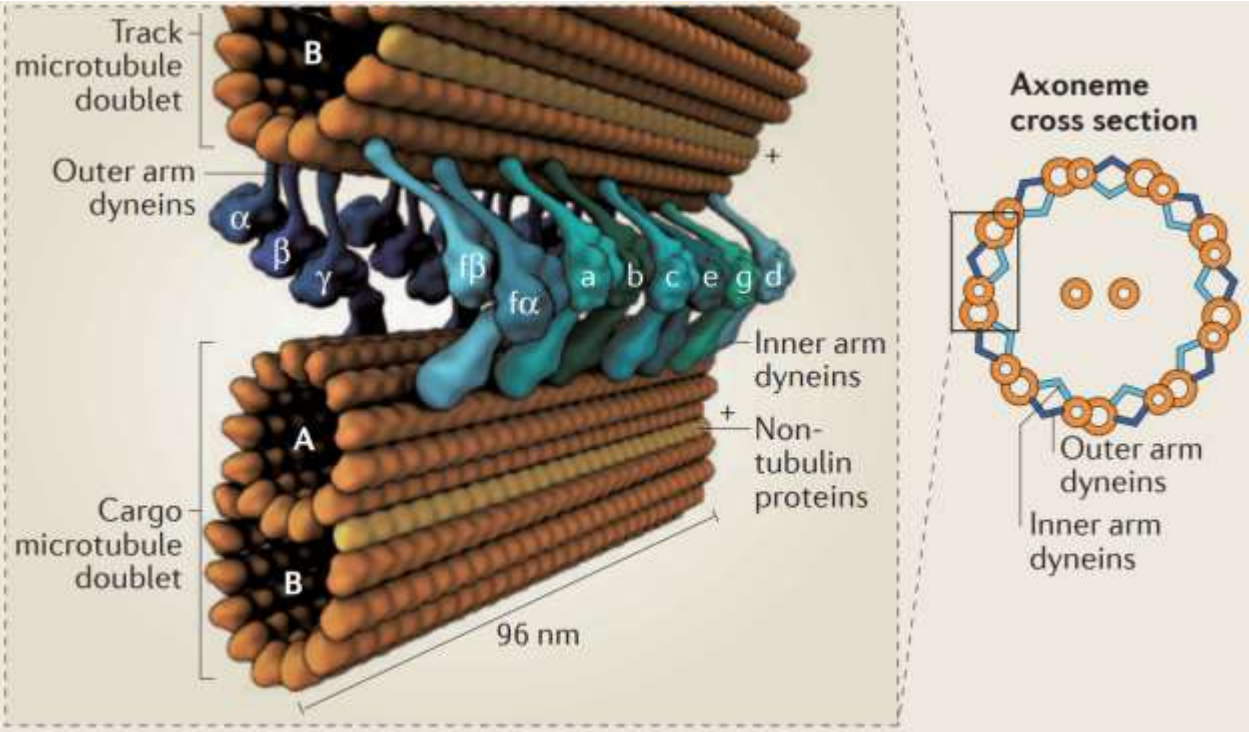

Fig. 3. Cross section of the '9 + 2' axoneme configuration showing the locations of the inner and outer arm dyneins. The A tubule of a microtubule doublet is a complete microtubule with 13 protofilaments while the B tubule of the doublet is an incomplete microtubule with 10 protofilaments. The polarity of the microtubules is indicated by plus signs.

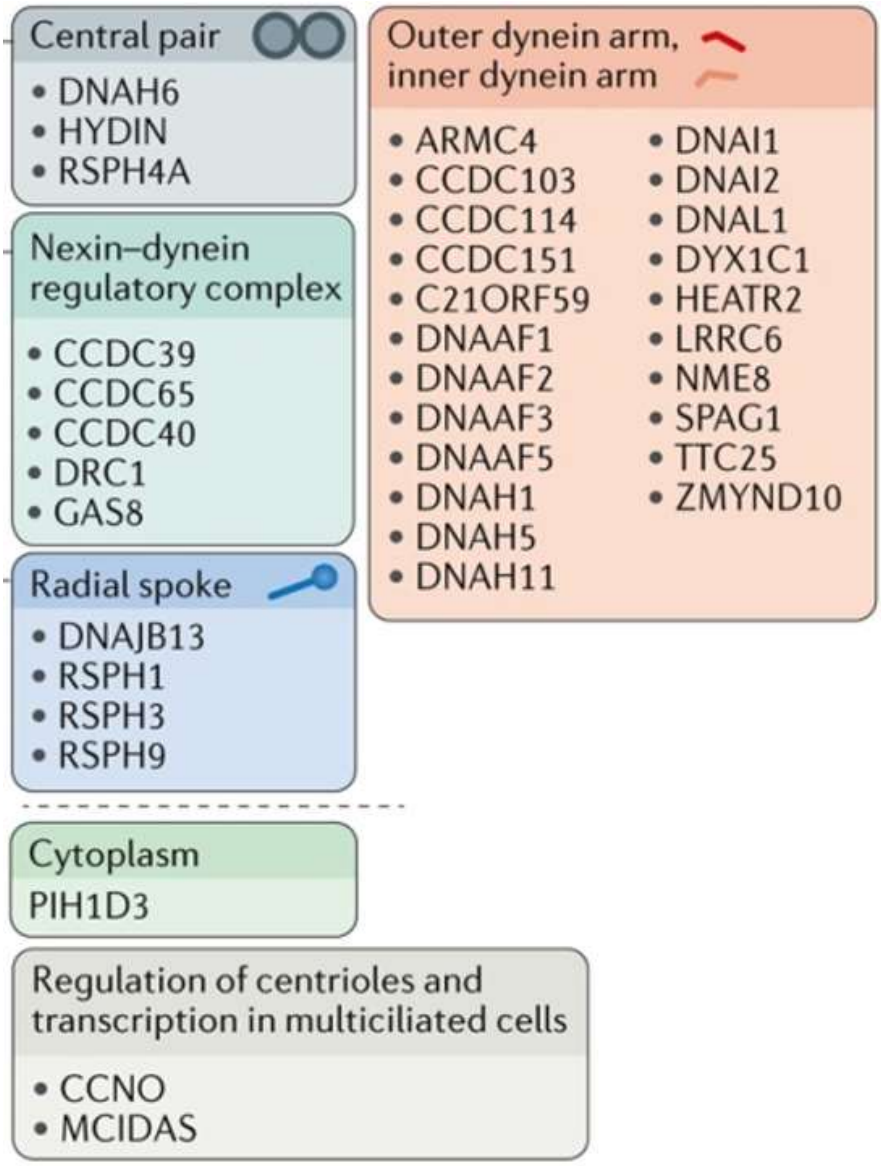

Fig. 4 Ciliopathy associated proteins in humans. Previous research has identified these proteins to be involved in the proper development of the key structures of cilia in humans and defects in the structure or functions of these proteins lead to ciliopathies. (Reiter & Leroux, 2017).

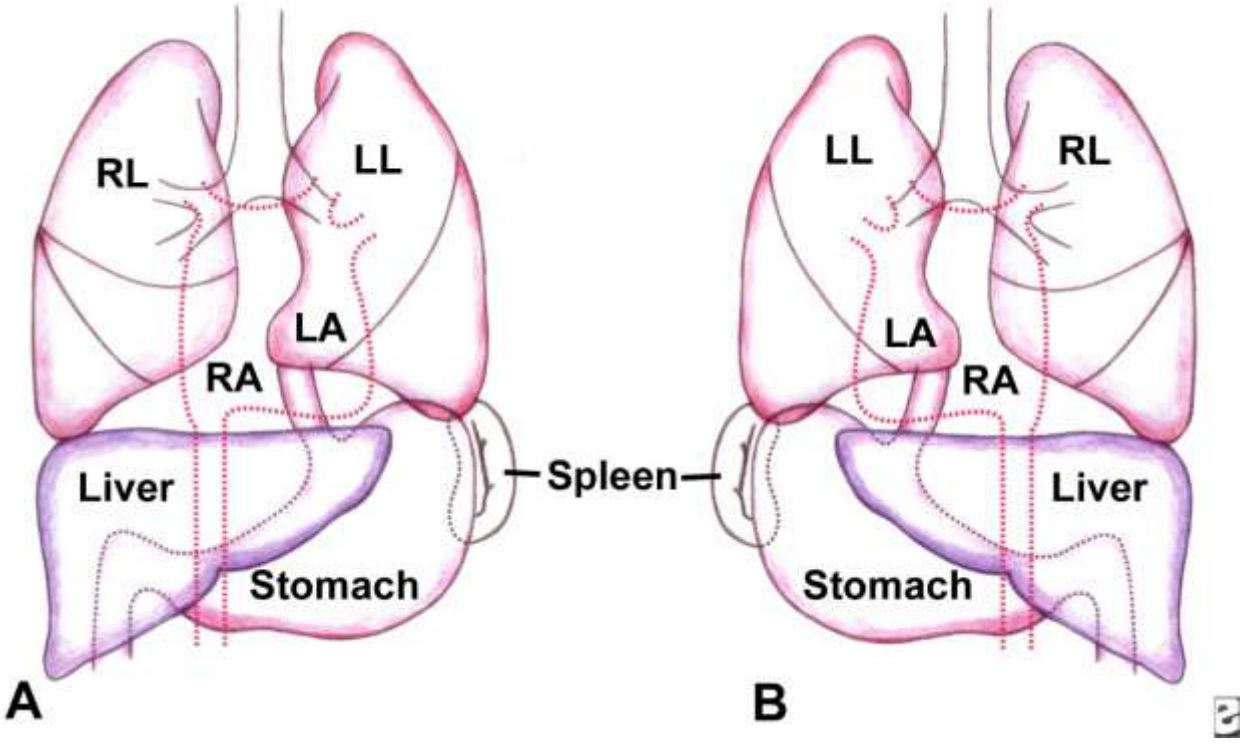

Fig. 5. ***situs inversus*.** A reversal of normal left-right asymmetry of the asymmetrically located visceral organs in the chest and abdomen. A, distribution of visceral organs with normal asymmetry. B, distribution of visceral organs in *situs inversus totalis*. RL, right lobe of the lungs; LL, left lobe of the lungs; LA, left atrium of the heart; RA, right atrium of the heart.

1.4 Human *LRRC56* is Homologous to the Algal *oda8* gene which is involved in the Cytoplasmic Pre-assembly of the Outer Dynein Arms.

Other than tubulin, the main component of microtubules, the outer dynein arms (ODAs) are the most abundant structural components in the axonemes of motile cilia (Desai et al., 2015). These ODAs have previously been reported to be reliant on the intraflagellar transport (IFT) machinery for their cytoplasmic pre-assembly and transport into the flagellar compartment (Hou et al., 2007; Ahmed, Gao, Lucker, Cole, & Mitchell, 2008). IFT is the bidirectional transport of multi-subunit protein complexes, called IFT particles, along axonemal microtubules beneath the ciliary membrane (Hao & Scholey, 2009). This bi-directional transport is carried out by two cytoskeletal motors: kinesin in the anterograde direction and the intraflagellar dyneins in the retrograde direction (Fig. 6) (Scholey, 2008). ODAs are assembled and mature in the cytoplasm of the cell outside of the cilia compartment (Omran et al., 2008; Horani et al., 2012). Therefore, they require the aid of transporters to get into the ciliary compartment. Through previous research many proteins involved in the cytoplasmic maturation and transport of the ODAs have been identified. These include IFT88 and IFT46, central components of the IFT machinery (Boehlke et al., 2015; Taschner, Mourão, Awasthi, Basquin, & Lorentzen, 2017), ODA5/ODA10, components of the ODA assembly complex (ODA AC) (Desai et al., 2015), ODA16, an adaptor for the ODA and IFT machinery (Taschner, Mourão, Awasthi, Basquin, & Lorentzen, 2017) and finally ODA8, another component of the ODA assembly complex (Desai et al., 2015; Dean & Mitchell, 2015).

In humans, loss of ciliary motility due to defects in ODA assembly have been associated with the development of PCD (Loges et al., 2008; Lobo, Zariwala, & Noone, 2014) demonstrated by respiratory infections and in approximately 50% of patients, laterality defects (including s*itus inversus totalis* and, less commonly, heterotaxy and congenital heart disease) (Leigh et al., 2009).

These defects in the ODAs or in their cytoplasmic pre-assembly, can be caused by errors in the genes that code for the dynein subunits themselves e.g. the dynein *ic76* gene (Pennarun et al., 1999), the axonemal docking sites on the microtubule doublets e.g. the *ccdc114* gene coding for a protein that is part of the ODA docking site on the axonemal microtubules (Onoufriadis et al., 2013), or the proteins involved in the pre-assembly and transport of the pre-assembled dyneins from the cytoplasm to the flagellar compartment e.g. IFT88/46, ODA5/10, ODA16, ODA8 as mentioned previously (Omran et al., 2008; Horani et al., 2012; Boehlke et al., 2015; Taschner, Mourão, Awasthi, Basquin, & Lorentzen, 2017; Taschner, Mourão, Awasthi, Basquin, & Lorentzen, 2017; Desai et al., 2015; Dean & Mitchell, 2015).

Recently, the algal *oda8* gene in *Chlamydomonas reinhardtii* was reported to be a Leucine Rich Repeat (LRR) gene homologous to the vertebrate *LRRC56* (Leucine Rich Repeat Containing 56) gene using RNA sequencing and RT-PCR coupled with the *in-silico* software phytozome (Desai et al., 2015). Through immunoprecipitation of ODA complexes that were pre-assembled in the cytoplasm of WT *Chlamydomonas reinhardtii* and *oda8* gene knockout mutants, it was discovered that the ODA complexes in *oda8* mutants had either not fully assembled or had assembled into complexes that partially dissociated during immunoprecipitation (Desai et al., 2015). Furthermore, the *LRRC56* gene was also reported to not be present in the genome of all organisms with motile cilia or flagella. Instead, LRRC56 homologs were lost both in species that did not have ODAs and in species that retained ODAs but that did not depend on IFT for axonemal assembly, supporting a role for LRRC56 in IFT-based dynein transport from the cytoplasm to the ciliary compartment (Desai et al., 2015). Therefore, the algal *oda8* gene was shown to be necessary for the cytoplasmic pre-assembly and transport of mature ODA complexes during flagellar assembly.

The *LRRC56* gene is a member of the vertebrate LRR gene family. Although other members of this gene family have been implicated in ciliopathies: *LRRC50* and *LRRC6* (Van Rooijen et al., 2008; Horani et al., 2013), the presence of the LRR protein motif does not indicate a possible role in cilia development. For example, the LRRC32 protein has been identified to be critical for tethering TGF-beta, a cytokine which is important in T-cell mediated immunology, to the surface of the cell (Tran et al., 2009). Again, LRRC8, another protein in the LRR family, is the main component of volume regulated anion channels which are activated in response to hypotonic stress from a cell's immediate environment (Voss et al., 2014; Deneka, Sawicka, Lam, Paulino, & Dutzler, 2018). These seemingly different roles of proteins in the LRR family are because the LRR motif is primarily involved in the formation of protein-protein interactions (Kobe, 2001), thus giving them a wide range of functionalities. Generally, LRR motifs are 20–29 residues long and contain a conserved 11-residue segment with the consensus sequence LxxLxLxx$^{N}/_{C}$xL where x can be any amino acid and L positions can also be occupied by valine, isoleucine and phenylalanine (Kobe, 2001). Furthermore, the number and location of LRR motifs vary between proteins in the LRR family. In humans, LRRC50 contains 6 LRR motifs located very close to its N-terminal region, LRRC6 contains 5 LRR motifs also located very close to its N-terminal region, LRRC32 contains a whopping 20 LRR motifs spread throughout the length of the protein, while LRRC56 contains just 4 LRR motifs once again located close to its N-terminal region.

In 2018, using human epithelial and *Trypanosoma brucei* cell lines, Dr. Boycott's group reported that the LRRC56 protein interacts with the intraflagellar transport (IFT) protein IFT88 during motile cilia formation and that mutations in the *LRRC56* gene results in severely dyskinetic cilia (Bonnefoy et al., 2018). These agree with the earlier findings in Desai et al., 2015, on the

interaction of *oda8* with the IFT machinery during outer dynein arm maturation in the alga *Chlamydomonas reinhardtii*.

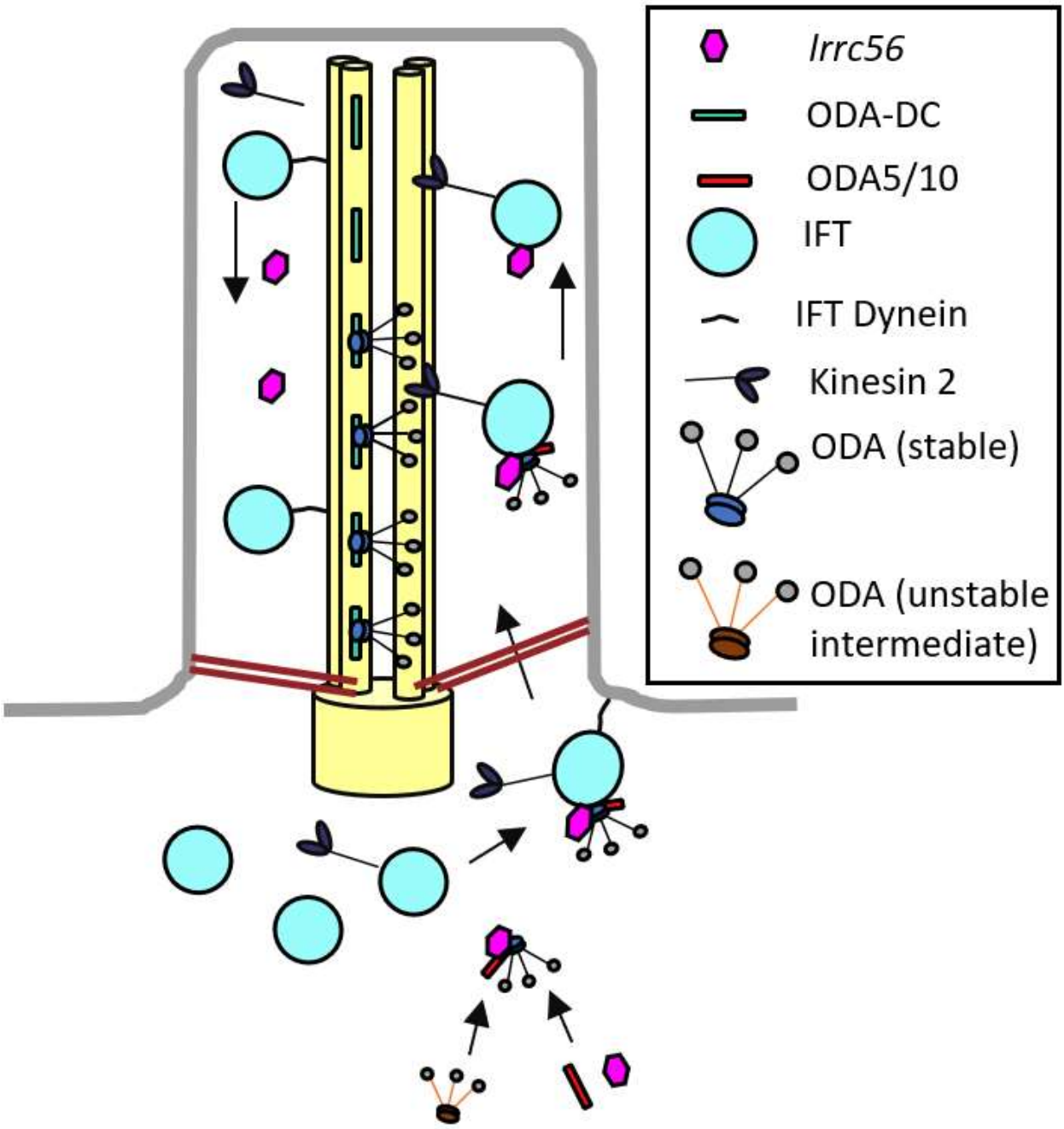

Fig. 6. Schematic of cytoplasmic ODA maturation and transport. Unstable ODAs bind to the ODA5/10 assembly complex and *lrrc56* for their cytoplasmic maturation. This complex of stable ODAs, ODA5/10 and *lrrc56* then bind to the IFT machinery for transport to the cilia compartment. The stable ODAs then bind to the ODA-DC on the A-microtubule doublet and the IFT machinery and *lrrc56* are released in the cilia compartment.

1.5 Zebrafish as a Model Organism

As earlier mentioned, two mutant fetuses which were identified at CHEO had *situs inversus* of thoracic and abdominal structures as well as complex cardiac anomalies, suggestive of a ciliopathy, possessed a homozygous missense variant of their *LRRC56* gene. The human *LRRC56* gene is 17.4 kilobase pairs (Kbp) in length, with 14 exons of which 11 are coding (Fig. 7A). It encodes a 542 amino acid (aa) protein that possesses four functional LRR motifs located close to the N-terminal region (Fig. 7B). In the fetuses, the missense mutation was in the 4th coding exon of their *LRRC56* genes. Structurally, this mutation affected the third LRR motif (Fig. 7B red star). Specifically, the mutation was identified to be p.Leu140Pro where a single nucleotide change from a thymine to a cytosine resulted in the Leucine at the 140th amino acid position being substituted for the amino acid Proline (Fig. 8). Because there were only two identified cases of this mutation, it was necessary to create an animal model to study the function of *LRRC56 in vivo* and confirm a link between the missense mutation of human *LRRC56* gene and the phenotypes observed in the fetuses.

Zebrafish (*Danio rerio*) exhibit many advantages as a disease model for human ciliopathies. To begin with, zebrafish embryos develop externally which allows them to be easily characterized and observed during early development. Due to the teleost-specific genome duplication event, the zebrafish genome contains many more genes compared to humans. However, a study reported that approximately 70% of human genes had a zebrafish orthologue, and more than 82% of human disease related genes described in the Online Mendelian Inheritance in Man (OMIM) database also have at least one zebrafish orthologue (Howe et al., 2013, Song et al., 2016). Furthermore, the successful adaptation of the CRISPR/Cas9 genome editing technology for zebrafish has promoted the use of zebrafish as a model for human ciliopathies caused by genetic mutations (Liu et al.,

2014). Finally, zebrafish have been used in many studies as a successful model for human ciliopathies (Austin-Tse et al., 2013; Schmidts et al., 2012; Mangos et al., 2010). For example, in 2007, zebrafish *lrrc50* knockout mutants were used to study a human ciliopathy: polycystic kidney disease. These zebrafish knockout mutants developed kidney cysts and impaired fluid flow in their pronephros, recapitulating phenotypes observed in the human condition. In addition, *situs inversus* of the visceral organs and curvature of the spine were also observed (Van Rooijen et al., 2008).

Zebrafish have a single copy of the *lrrc56* gene 9.7kb in length with 11 coding exons (Fig. 7C) translating to a protein of 607aa. Unlike the human *LRRC56* with 4 LRR motifs, the zebrafish *lrrc56* gene possesses five LRR motifs located close to the N-terminal region of the protein (Fig. 7D). An amino acid sequence comparison of the human and zebrafish Lrrc56 proteins showed that the fifth LRR functional domain found in the zebrafish Lrrc56 protein does not exist in its human counterpart. In terms of homology, overall, the zebrafish Lrrc56 protein is 40.5% identical to its human counterpart but has a 64% similarity in the region of the LRR domains. The Leucine at the 140^{th} aa position that is converted to Proline in the human fetuses is conserved and located in the third functional LRR motif (Fig. 7D red star) at the end of the fourth exon of the zebrafish *lrrc56* gene (Fig. 8).

Considering the multiple advantages of using zebrafish as an animal model for human diseases and the homology between the *lrrc56* gene in zebrafish and the human *LRRC56* gene, we decided to generate zebrafish *lrrc56* gene mutants using the CRISPR/Cas9 genome editing technology and to characterize their development.

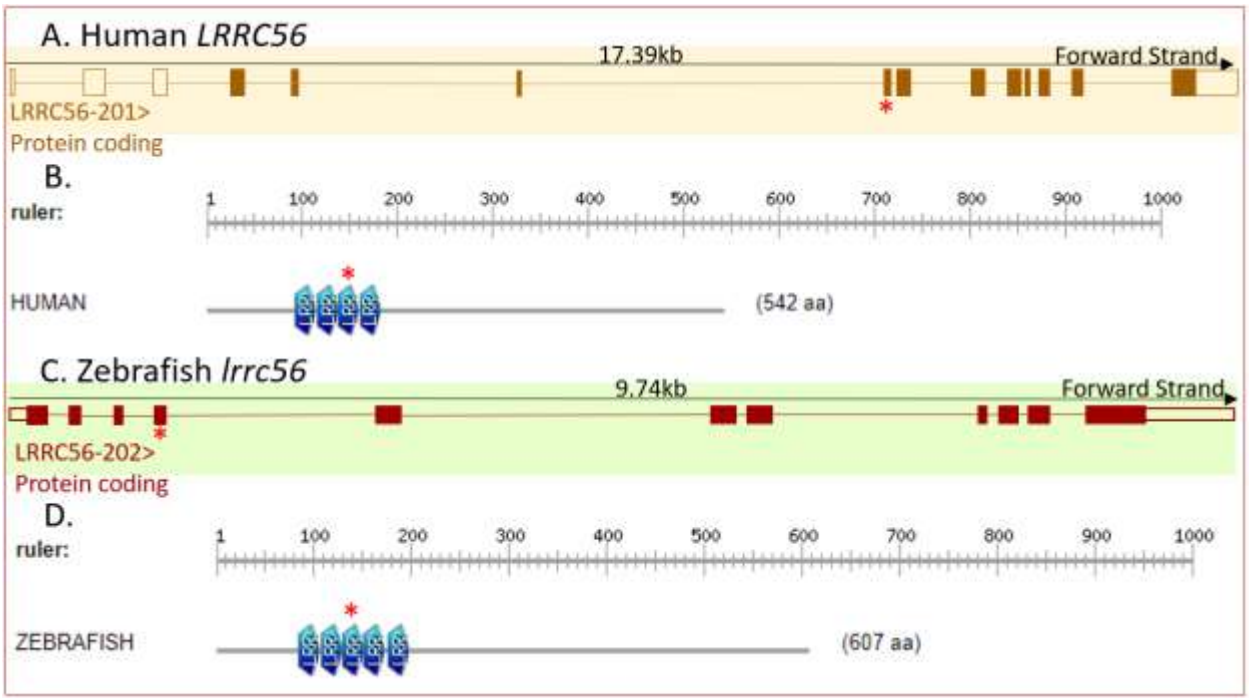

Fig. 7. LRRC56 gene in Zebrafish and Humans. The red stars indicate the locations of the missense variant observed in the fetuses. The sizes of the boxes and lines in this figure represent the approximate sizes of the exons and the introns and the distance between each exon. A, schematic of the human *LRRC56* gene. Each filled in box in the schematic represents an exon for a total of 11 coding exons. The un-filled boxes at the 5' end of the gene represent the 3 non-coding exons while the unfilled in box at the 3' end represents the 3' untranslated region (UTR). The lines in between the boxes represent the introns. B, the human LRRC56 protein possesses four LRR domains close to its N-terminal region. C, schematic of the zebrafish *lrrc56* gene. Each filled in box in the schematic represents an exon for a total of 11 coding exons. The un-filled box at the 5' end of the gene represents the 5' UTR while the unfilled in box at the 3' end represents the 3' UTR. The lines in between the boxes represent the introns. D, the zebrafish Lrrc56 protein possesses five LRR domains close to its N-terminal region.

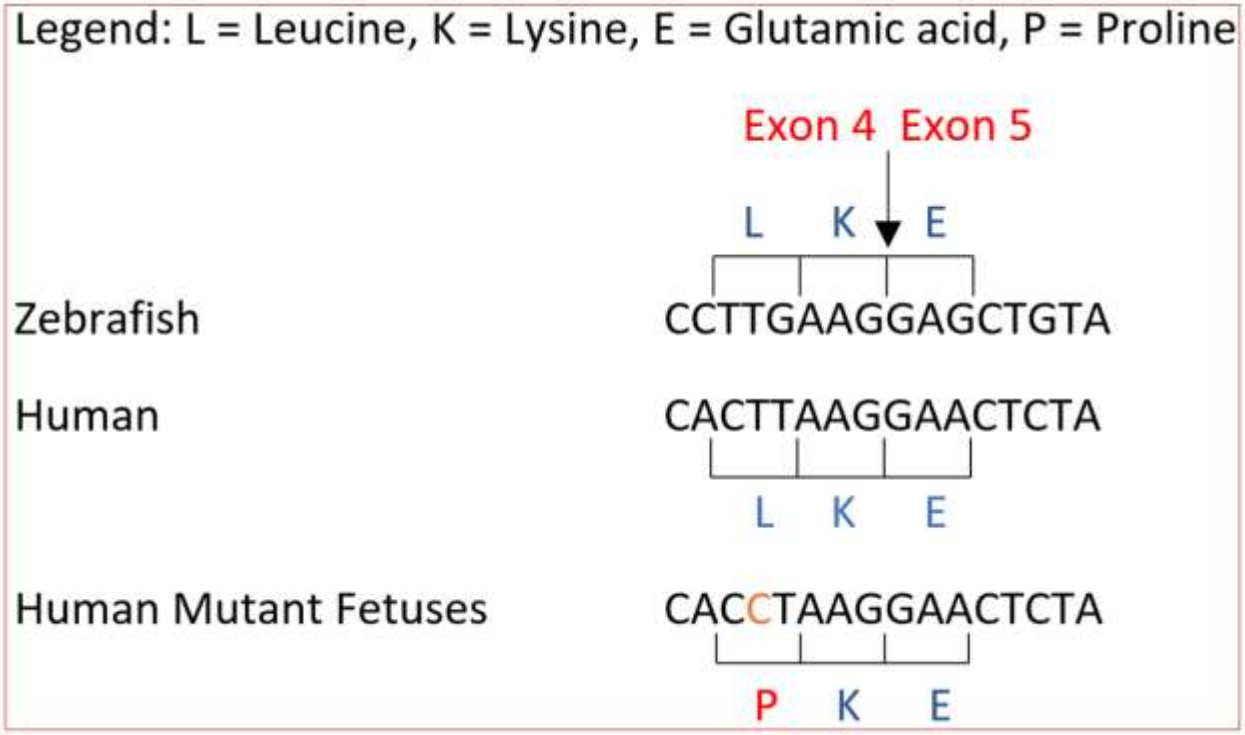

Fig. 8. Schematic of p.Leu140Pro. Sequence comparison of the location of the LRRC56 gene homozygous missense variant in the human mutant fetuses vs in humans and zebrafish. Letters in blue denote the wild-type amino acid while the letter in red denotes the mutant amino acid. The letter in orange denotes the nucleotide responsible for the amino acid change at the 140th aa position from Leucine to Proline.

1.5.1 Cilia and Determination of Asymmetry in Zebrafish

Motile cilia can be found in many zebrafish organs including the olfactory node, pronephric duct, ventral spinal cord and the Left Right Organizer (LRO) (Malicki, Avanesov, Li, Yuan, & Sun, 2011). Motile cilia found in zebrafish generally possess the "9+2" microtubule structure except for those found in the spinal cord, where motile cilia with the "9+0" and "9+2" structures both exist (Kramer-Zucker, 2005; Sarmah, Winfrey, Olson, Appel, & Wente, 2007; Song et al., 2016).

Like humans, zebrafish are outwardly bilaterally symmetric and organs like the heart, liver and gut are also asymmetrically located. The physical locations of these organs in a zebrafish are determined very early during its development (Matsui & Bessho, 2012). Previous studies have shown that there are four stages to the determination (Fig. 9.) of left-right asymmetry in zebrafish (Matsui & Bessho, 2012). The first stage is a bilateral symmetry breaking stage that occurs even before the start of zygotic transcription in zebrafish embryos. This stage was discovered when embryos between the 2-cell and 64-cell stages, treated with H^+/K^+-ATPase inhibitors, displayed randomized phenotypes indicative of LR patterning defects (Kawakami, Raya, Raya, Rodríguez-Esteban, & Belmonte, 2005).

The second stage is the Dorsal Forerunner Cells (DFCs)/Kupffer's Vesicle (KV) organogenesis stage (Essner et al., 2002). The Kupffer's Vesicle is the LRO in zebrafish and while it is conserved among teleost fishes (Brummett & Dumont, 1978), it is also functionally and structurally homologous to the LRO found in vertebrates (Schneider, Houston, Rebagliati, & Slusarski, 2007). In zebrafish embryos, the KV is a fluid-filled epithelial sac that exists transiently between 9 and 14 hours post fertilization (hpf) during early zebrafish development at the posterior end of the tail bud in zebrafish (Fig. 10). Electron microscopy with the fish *Fundulus heteroclitus*, showed that a single cilium (monocilium) extends from each cell lining KV into the lumen (Brummett &

Dumont, 1978). The KV is formed from a group of approximately twenty-four cells known as the DFCs (Essner, 2005). Although KV was first described more than 100 years ago, it is still unknown whether the DFCs and the KV are mesodermal or endodermal in origin (Warga & Stainier, 2002). With the aid of the motile monocilia generated from each DFC, whose axonemes are arranged in the '9+2' formation (Babu & Roy, 2013), the fluid flow in the KV is driven in a counter-clockwise direction (Essner, 2005). This counter-clockwise flow restricts the expression of *southpaw*, a nodal-related gene, to the left side of the zebrafish lateral plate mesoderm (LPM) as one of the earliest steps to determining L/R asymmetry (Long, Ahmad, & Rebagliati, 2003). The *NODAL* gene is responsible for the determination of L/R asymmetry in vertebrates (Shen, 2007). In zebrafish, there are three nodal-related genes: *southpaw, squint, cyclops*, but only *southpaw* influences L/R patterning (Baker, Holtzman, & Burdine, 2008).

After the KV organogenesis stage, the next stage is the lateral plate mesoderm (LPM) stage (Long, Ahmad, & Rebagliati, 2003). In this stage, the restricted left sided expression of *southpaw* in the LPM stimulates the further expression of *southpaw* in the left LPM and its inhibitor *lefty1* along the midline (Long, Ahmad, & Rebagliati, 2003). *lefty1* acts as a nodal inhibitor and ensures the continual restriction of *southpaw* in the left LPM (Smith et al., 2011; Long, Ahmad, & Rebagliati, 2003). This continual expression of *southpaw* results in a genetic cascade, which is crucial for the transfer of directional L/R asymmetric information into the organ primordia (Matsui & Bessho, 2012).

Finally, the last stage is the left-right (L/R) specific organ morphogenesis stage (Matsui & Bessho, 2012). In this stage, the left-sided *southpaw* signals in the LPM are eventually relayed to the organ primordia which then leads to left-specific organ morphogenesis evidenced by Long, Ahmad, & Rebagliati, 2003 reporting that a knockdown of *southpaw* in *Tg[lefty1::GFP]*, a transgenic line

that can report nodal related activity in zebrafish, resulted in the loss of left-sided activation of Nodal signaling in the diencephalon. Visceral organs like the heart, liver and gut use laterality signals generated by the monocilia driven leftward fluid flow in the KV to determine their locations during development. The zebrafish heart undergoes two distinct asymmetric events: cardiac jogging and cardiac looping. Cardiac jogging in zebrafish is the process by which the symmetrical zebrafish heart tube is displaced relative to the dorsal midline, with a leftward 'jog' in the WT condition (Khodiyar, Howe, Talmud, Breckenridge, & Lovering, 2013) and can be observed in zebrafish at 24 hpf. On the other hand, cardiac looping which can be observed in zebrafish at 36hpf, is what occurs when the initially straight embryonic heart tube becomes transformed into a helically wound loop that is normally seen with a counterclockwise winding (Männer, 2009). The liver bud undergoes just one asymmetric positioning event where by 30 hpf, the liver bud emerges on the left side of the zebrafish larva from a dorsal view (Grimes & Burdine, 2017). Laterality defects can be detected by the analysis of the expression of genes specific to each visceral organ. For example, by analysing the expression of the zebrafish cardiac myosin light chain-1 (*cmlc1*) in the heart, the position of the heart in zebrafish can be identified.

Due to our interest in cilia, we will only be looking at two of these stages: the DFCs/KV stage where monocilia play a major role and the L/R specific organ morphogenesis stage which allows us to directly analyze and identify the roles of the cilia and the *lrrc56* gene in determining organ asymmetry.

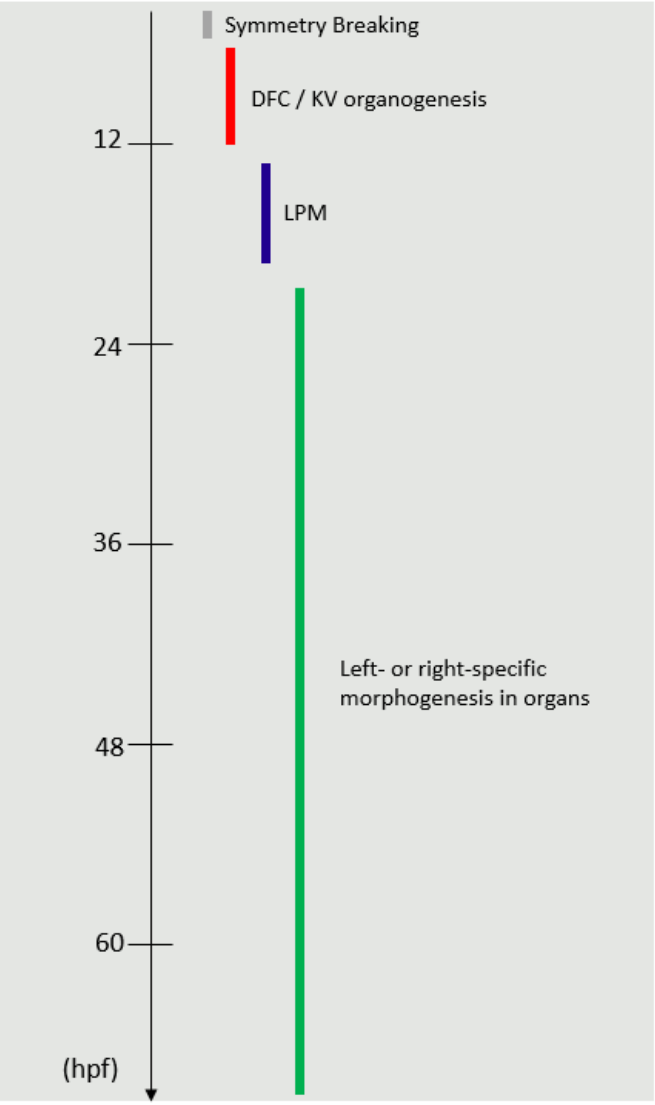

Fig. 9. Stages of L/R asymmetric determination in patterning in zebrafish. A symmetry-breaking process occurs by 3 hpf. The LRO called the Kupffer's vesicle (KV) is formed by 12 hpf and generates a counterclockwise fluid flow to create an L/R difference in *southpaw* around the KV. Asymmetric signals are then transferred from the KV to the LPM. The Left- or right-specific morphogenesis then occurs in organs later during development.

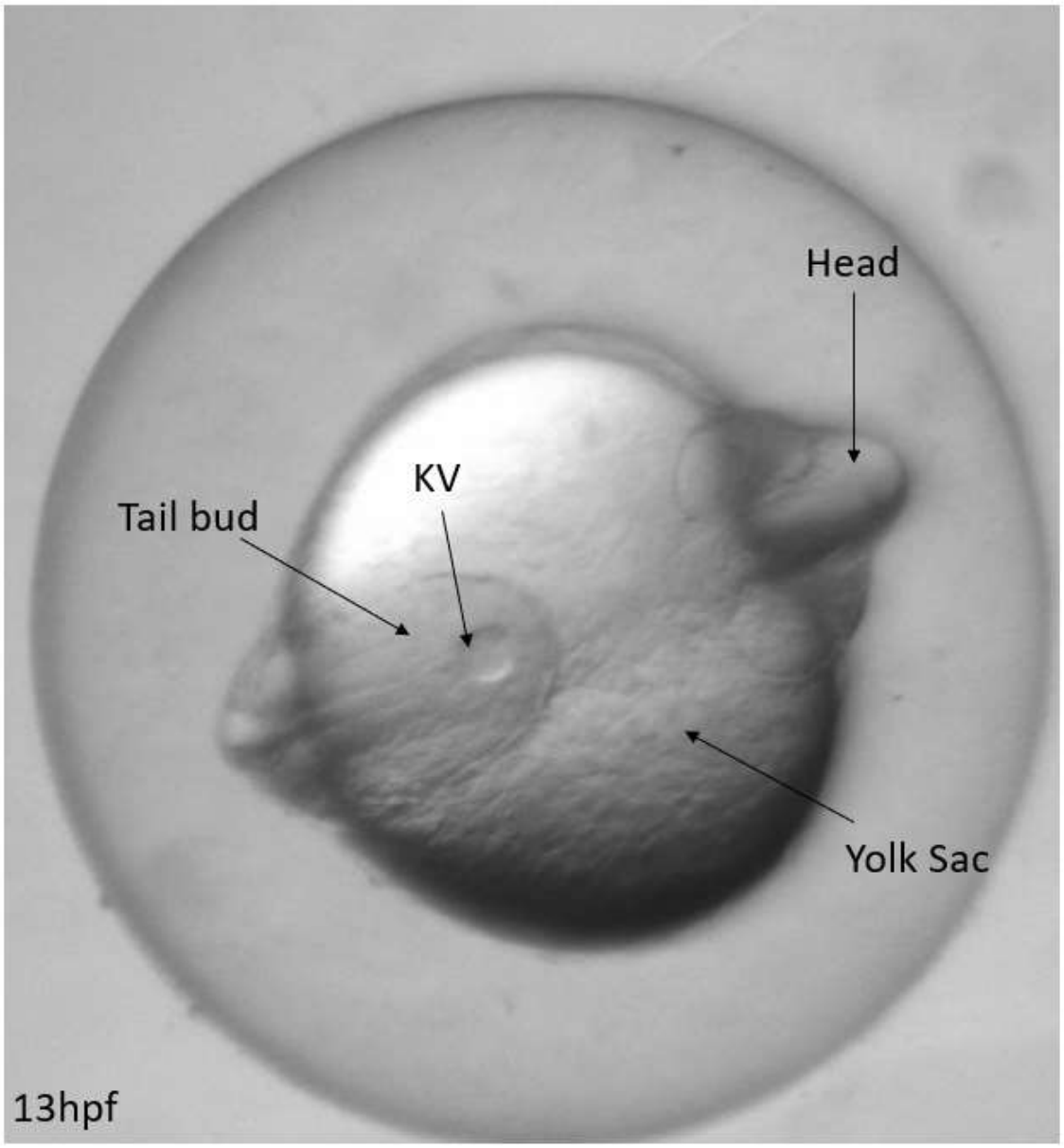

Fig. 10. Ventral view of a Zebrafish embryo at 13 (hpf) showing the location of the KV.

1.6 CRISPR/Cas9 Targeted Genome Editing

In bacteria, the Clustered Regularly Interspaced Short Palindromic **r**epeats (CRISPR) and the CRISPR-Associated (Cas) 9 genes are necessary in the development of sequence-specific adaptive immunity against invading genetic material (Richter et al., 2012). This system functions by using CRISPR RNA (crRNA) guided Cas9 nucleases to introduce double strand breaks in foreign DNA, essentially destroying them (Jinek et al., 2012). The RNA guided Cas9 nucleases from the microbial CRISPR-Cas systems have been adapted to cause targeted double-stranded DNA breaks (DSBs) in eukaryotic cells at a target site (Cong et al., 2013). Due to the DSBs, the non-homologous end-joining (NHEJ) or homology-directed repair (HDR) cellular repair mechanisms are activated, which could then induce error-prone alterations in the case of NHEJ or defined alterations in HDR (Ran et al., 2013) (Fig. 11). The double stranded DNA endonuclease activity of the Cas 9 protein has a requirement that a short-conserved sequence having a length between 2 and 5 nucleotides called the Protospacer Adjacent Motif (PAM) follows immediately downstream of the crRNA complementary sequence of 20 nucleotides known as the protospacer (Swarts et al., 2012). Without the PAM, sequences that are complementary to the crRNA guided Cas9 are ignored (Sternberg et al., 2014). To obtain site-specific DNA recognition and cleavage, Cas 9 must be complexed with both a crRNA and a separate trans-activating crRNA (trRNA), which is partially complementary to the crRNA (Jinek et al., 2012). This trRNA is necessary for the maturation of the crRNA from a primary transcript that encodes multiple pre-crRNAs (Deltcheva et al., 2011). Based on this system, the trRNA and the crRNA have been combined into a simplified synthetic single guide RNA (sgRNA) (Fig. 8) and this simplified combination with Cas9 has been shown to be just as effective as a Cas9 protein with trRNA and crRNA in guiding gene alterations

(Jinek et al., 2012). Gene knockouts via CRISPR/Cas9 genome editing is based on the NHEJ mechanism.

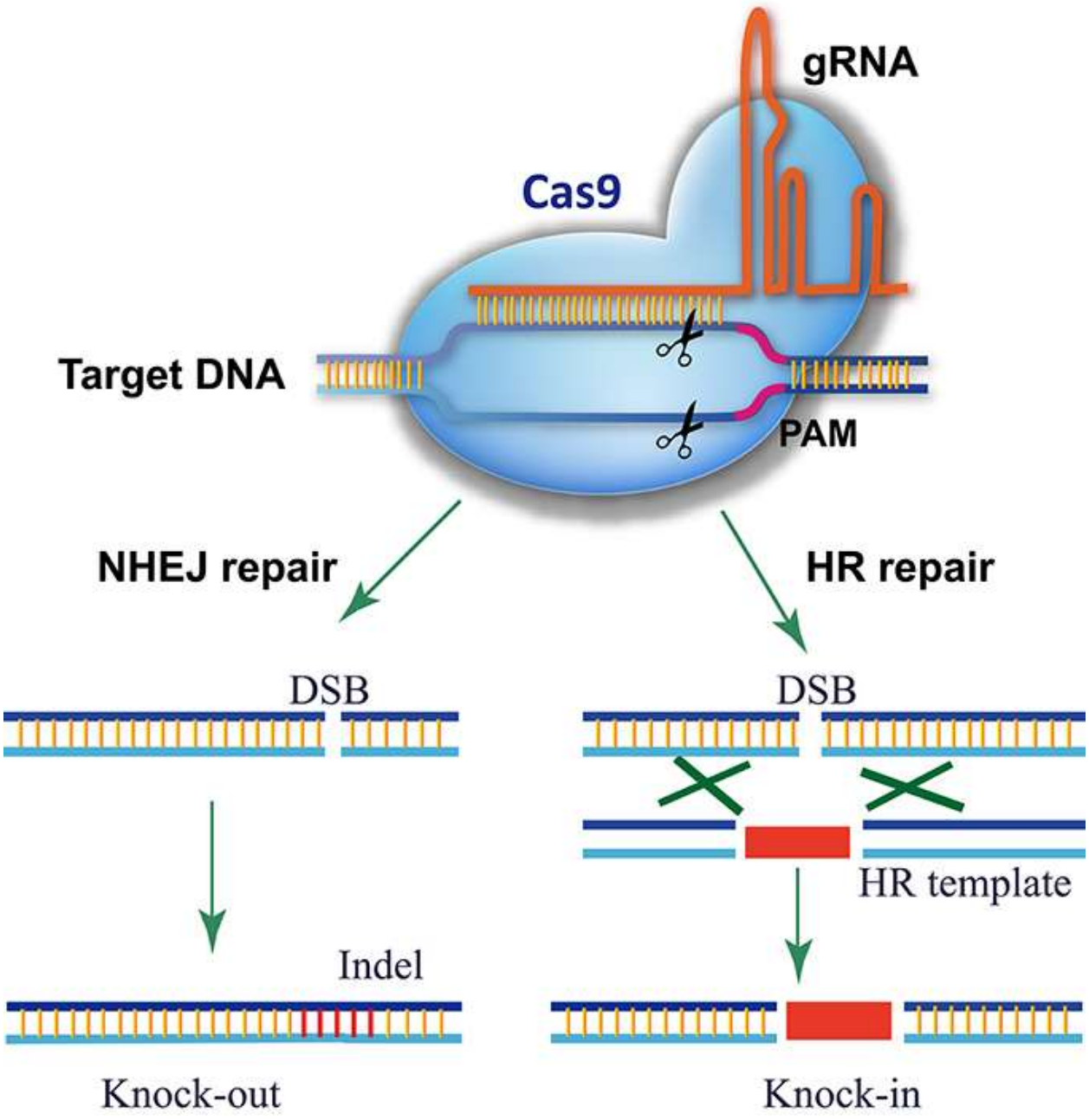

Fig. 11. Schematic of DNA cleavage by CRISPR genome editing. The simplified gRNA is complexed with the Cas9 protein to cause DSBs in the target DNA sequence which are then repaired either through the non-homologous end joining or homology directed repair mechanisms.

1.7 Project Objectives

To study the *in vivo* function of the *LRRC56* gene and confirm a link between the human *LRRC56* gene and the phenotypes observed in the autopsied fetuses at CHEO, we used the CRISPR/Cas9 genome editing technique to modify the genome of zebrafish embryos with the CRISPR/Cas9 genome editing technique. Although the fetuses possessed a homozygous missense variant p. Leu140Pro of the *LRRC56* gene, replicating this mutation involves a "knock-in" using CRISPR homology directed repair which is currently a challenge in zebrafish. Therefore, in a first approach we decided to knockout the zebrafish *lrrc56* gene and analyze the resulting zebrafish mutants. We therefore hypothesized that if the mutation of the *LRRC56* gene in the human fetuses renders the lrrc56 protein inactive, a knockout of the zebrafish *lrrc56* gene might produce in zebrafish similar phenotypes to those observed in the mutant human fetuses. This hypothesis led to the two objectives of this project:

- Create homozygous zebrafish *lrrc56* gene knockouts.
- Characterize the resulting phenotypes in the homozygous *lrrc56* knockout zebrafish.

Since this mutation observed in the fetuses is an autosomal recessive mutation and in both fetuses the phenotypes were observed with a homozygous missense variant, we predicted that the mutant phenotypes should only be observed in the homozygous *lrrc56* knockout mutants and not in the heterozygous *lrrc56* mutants. Finally, if the *lrrc56* gene is indeed involved in the process of cilia maturation, we expected to observe ciliopathy associated phenotypes like L/R asymmetry in the homozygous zebrafish embryos.

2.0 Materials & Methods

2.1 Ethics Statement

Zebrafish were handled according to guidelines provided by the Canadian Council on Animal Care and protocols approved by the University of Ottawa Animal Care Committee (approval ID: BL-2589). Experiments involvingObservers involved in the experiments were blinded to the phenotypes of the zebrafish but were not blind to the genotypes of the zebrafish they observed.

2.2 Zebrafish Maintenance

Zebrafish were kept in tanks or smaller breeding traps at 28.5^{o}C with a 14h light cycle and a 10h dark cycle from lights-on at 9:00AM till lights-off at 11:00PM. Embryos obtained from crosses were bleached between 5 to 28 hours post fertilization (hpf). These embryos were raised till 7 days post fertilization (dpf) in plastic petri dishes inside an incubator kept at 28.5^{o}C. From 1dpf to 6dpf, zebrafish embryos were kept in system water containing methylene blue. From 6dpf till the end of the experiments, the zebrafish were kept in only system water. Housing of zebrafish was limited between 30 – 60 adult individuals in 10L of system water or 10 – 20 adults in 3L of system water.

Feeding: Zebrafish larvae were fed with ~15 mg of Gemma75 per day and 50 ml of fresh water was added every day. Food quantities were gradually increased as the larvae developed. Juveniles and adults were then fed Gemma150 and Gemma300, respectively. To prevent melanin formation in embryos older than 24 hpf for experimental purposes, PTU (1-phenyl 2-thiourea, 0.3 mg/ml) was supplemented to fish water at 9 hpf until the embryos were sacrificed.

2.3 Genotyping

lrrc56 gene mutant zebrafish were genotyped using a heteroduplex analysis assay (HAA) as described in Zhu et al., 2014. To extract genomic DNA from embryos, 100µl of 50mM NAOH

(sodium hydroxide) was first added to a pool of ten randomly selected embryos. Next, the embryos in NAOH were heated at 95ºC for 10 minutes and then cooled at 4ºC for 5 minutes. Finally, 10µl of 1M Tris-HCL pH 8.0 was added to the mixture of the embryos and NAOH. This final mixture contained the genomic DNA that was used for genotyping (Meeker, Hutchinson, Ho, & Trede, 2007). Primers flanking the CRISPR target site (forward sequence: "LT1 Forward", 5'-GACCTGGCACAACTCACTCC-3', reverse sequence: "LT1 Reverse", 5'-GTGTGGATTTTC ACCCATGA-3') were used to amplify a DNA fragment of 245bp. The program used for the thermal cycler PCR amplification started with an initial denaturation step of 5 minutes at 95°C. Next, the thermal cycler cycled through the following steps 24 times: a 30 second denaturation step at 94°C, a 30 second annealing step at 58°C and a 30 second elongation step at 72°C. The amplification program then ended with a final 5-minute elongation step at 72°C. Afterwards, the PCR reaction was kept at 22ºC.

Since the resulting PCR amplicons were expected to contain either mutant or WT alleles, the amplicons were denatured at 95ºC for 5 minutes and allowed to re-anneal at 4ºC for another 5 minutes to allow the formation of homoduplex and heteroduplex DNA that can be easily identified on a Polyacrylamide gel electrophoresis (PAGE) gel run with either a GeneRuler 50 bp or 100bp DNA ladder (Thermofisher) at 150V, 2.0A for 70 minutes and then stained with 15µl of RedSafe™ (20000X, FroggaBio) in 50µl of a 1X Tris/Borate/EDTA (TBE) buffer. The 1X TBE buffer was obtained by diluting a 5X TBE buffer (216g of Tris base, 110g of Boric acid, 80mL of 0.5M EDTA pH 8.0 in 4L of water).

Adult *lrrc56* zebrafish mutants were identified by HAA-PAGE using genomic DNA extracted from caudal fin clippings by once again immersing the fin clippings in 100µl of NAOH, heating the immersed fin clips at 95ºC for 10 minutes, letting the heated mixture cool at 4ºC for 5 min and

then adding 10µl of 1M Tris-HCL pH 8.0 to the cooled down mixture. The DNA of the *lrrc56* mutant zebrafish were sequenced at the Ottawa Hospital Research Institute (OHRI) to identify the specific mutations they possessed.

2.4 Whole mount *in-situ* hybridization

In situ hybridization (ISH) on whole mount zebrafish embryos were performed for a minimum of three biological replicates as previously described in Thisse & Thisse, 2007 with modifications. Zebrafish embryos were fixed in 4% paraformaldehyde (PFA) overnight at 4^{o}C and stored at -20^{o}C until use. On the 1st day, embryos were permeabilized with 0.01mg/ml of ProteinaseK (Invitrogen) in 1X Phosphate Buffered Saline with Tween20 (PBST) for 15 minutes at room temperature (RT) if they were older than 24 hpf. If they were 48 hpf or older they were permeabilized for 30 minutes. The embryos were then fixed in 4% PFA for 20 minutes at RT and acetylated with an acetylation mix (37.5µl triethanolamine, 8.1µl acetic anhydride in 3µl of diethyl pyrocarbonate (DEPC) treated water) for 10 minutes at RT. Afterwards the embryos were incubated in 700µl of a hybridization buffer (5ml of 100% de-ionized formamide, 2.5ml of 20X Saline Sodium Citrate (SSC) (3M sodium Chloride, 300mM trisodium citrate [adjusted to pH 7.0 with HCl]) buffer, 10µl of 100% Tween-20, 92µl of 1M Citric acid, 2.398ml of DEPC treated water, 50µl of 10mg/ml of yeast tRNA, 1µl of 50mg/ml of heparin) for 2 hours at 70^{o}C and 200µl of the hybridization buffer containing ~1ng/µl of anti-sense RNA probe at 70^{o}C overnight. On the 2nd day, embryos were washed at 70^{o}C in successive solutions: 75% hybridization buffer and 25% 2X SSC for 10 minutes, 50% hybridization buffer and 50% 2X SSC for 10 minutes, 25% hybridization buffer and 75% 2X SSC for 10 minutes, 2X SSC for 10 minutes, and twice in 0.2X SSC for 30 minutes. The embryos were then washed at RT in 75% 0.2X SSC and 25% PBST for 5 minutes, 50% 0.2X SSC and 50% PBST for 5 minutes, in 25% 0.2X SSC and 75% PBST for 5 minutes and in 100% PBST for 5 minutes. These embryos were then blocked for 1 hour at RT with 10% Calf Serum and 10mg/ml Bovine Serum Albumin in PBST and incubated with Anti-

digoxigenin-AP Fab Fragments (Roche – cat # 1093274) at 1:1000 overnight at 4°C. On the 3rd day, embryos were first washed at RT in PBST 6 x 15 minutes and then incubated in staining buffer (100 mM Tris HCl pH 9.5, 50 mM $MgCl_2$, 100 mM NaCl, 0.1% tween-20) 3 x 5 minutes. Embryos were then stained with 14µl of 5-Bromo-4-chloro-3-indolyl phosphate (BCIP) and 18µl Nitro Blue Tetrazolium (NBT) in 4ml of staining buffer at RT. Afterwards, to stop the staining reaction, the embryos were washed 3 x 15 min in PBST with 1mM EDTA at RT.

2.5 Probe Synthesis

Digoxigenin-labelled (DIG) RNA probes were transcribed with RNA polymerases using the cDNA plasmid templates listed in Table 2.1. 10µg of the cDNA plasmid template was linearized using enzymatic digestion with the proper restriction endonuclease for 2 hours at 37°C. The linearized plasmid was then purified using a GE Healthcare Illustra™ purification kit. The transcription reaction mix contained 1µl of the linearized cDNA template, 2µl of DIG labelling mix (10mM ATP, CTP, GTP, 6.5mM UTP and 3.5mM DIG-11-UTP) (Roche - cat # 1209256), 2µl of 10X transcription buffer (Roche), 0.5µl of RNase Inhibitor (Fermentas), 2µl of the appropriate RNA polymerase and 12.5µl of DEPC treated water. This mix was then incubated at 37°C for 2 hours. The RNA probes were isolated and purified using a SigmaSpin Post-Reaction Clean-Up Columns (Sigma-Aldrich) and stored at - 80°C

Probe	Vector	Restriction Enzyme	RNA Polymerase
cmlc1	pDrive	EcoRI	SP6
Anti-sense *lrrc56*	pDrive	BamHI	SP6
sense *lrrc56*	pDrive	HindIII	T7
foxA3	pCR4-TOPO	NotI	T3

Table 2.1 RNA probes for whole mount ISH

2.6 Bone and Cartilage staining with Alizarin Red and Alcian Blue

On the 1st day, 21 dpf zebrafish were fixed in 4% PFA overnight at 4°C. On the 2nd day, the fixed zebrafish were dehydrated in a solution of 50% ethanol, 50% water for 10 minutes. Afterwards, the zebrafish were stained in acid-free solution (10µl of 0.5% alizarin red dissolved in water added to a 1ml solution containing 0.02% alcian blue, 60mM $MgCl_2$, and 70% ethanol) at RT in the dark overnight. On the 3rd day, the zebrafish were first washed with water then bleached in a solution of 1.5% hydrogen peroxide (H_2O_2) and 1% potassium hydroxide (KOH) at room temperature for 20 minutes while exposed to the air. Afterwards the zebrafish tissues were cleared in 25% glycerol and 0.25% KOH overnight at room temperature. On the final day, solution was changed to 50% glycerol and 0.25% KOH. The zebrafish were viewed and imaged in this solution of 50% glycerol and 0.25% KOH under the microscope.

2.7 Immunohistochemistry (IHC)

Embryos were fixed overnight in 4% paraformaldehyde at 4°C. Fixed embryos were washed with PBST (containing 0.1% Tween-20) and incubated in acetone for 10 minutes at -20°C. The embryos were subsequently blocked in 1X Phosphate Buffered Saline (PBS) with 10% Calf Serum and 0.5% TritonX-100 for one hour. Embryos were incubated in mouse alpha Tubulin antibody (GenScript – cat # A01410, 1:250) either at 3 hours at RT or at 4°C overnight. After washing excess primary antibody in PBST, embryos were incubated in goat anti-mouse Alexa Fluor 594 (ThermoFisher - Catalog # A-11005, 1:500) either for 3 hours at RT or at 4°C overnight. Embryos were then washed in a 1:1000 dilution of 4,6-diamidino-2-phenylindole (DAPI) in PBST to label cell nuclei for 10 minutes and then washed with PBST for 30 minutes. After washing in PBST, embryos were mounted in 1% low melting point agarose and imaged using a Nikon A1R MP^+

confocal microscope with an Apo LWD 25x objective. Cilia length was measured using Simple Neurite Tracer® in Fiji.

2.8 RNA Extraction

Total RNA was extracted from a pool of fifty 2dpf WT or *lrrc56*$^{-/-}$ embryos using Trizol® Reagent (Invitrogen Cat # 15-596-018). This pool of embryos was homogenized in 1ml of Trizol buffer by vigorous mixing using a pipette. The homogenized sample was then incubated for 5 minutes at RT. 0.2ml of Chloroform was added to the homogenized sample and vortexed for 15 seconds. The sample was then incubated at RT for 3 minutes before being spun for 10 minutes at RT with 12500 Revolutions per minute (RPM). Subsequently, the resulting aqueous phase was isolated and 0.5ml of isopropanol was added to precipitate the RNA. The isolated aqueous phase with isopropanol was incubated for 10 minutes at RT before being spun at 4ºC for 15 minutes with 12500 RPM to obtain the RNA pellet. Afterwards, the RNA pellet was washed with 500µl of 75% Ethanol and spun for 5 minutes at 4ºC with 10000RPM. The RNA pellet was then resuspended in 20µl of RNAse-Free water and incubated at 55ºC for 10 minutes before being stored at -80ºC.

2.9 Reverse-Transcriptase Polymerase Chain Reaction (RT-PCR)

complementary DNA (cDNA) was synthesized from 1µg of total RNA extracted from zebrafish embryos using the QuantiTect Reverse Transcription Kit (Qiagen). PCR was then performed using the cDNA reaction mix as the DNA template. Next, 25µL reactions were prepared according to the GoTaq® Green Master Mix (Promega) protocol using custom primers designed to target a 197base pair (bp) region of the *lrrc56* gene and a 116base pair region for the human *β-globin* control as listed in Table 3. The RT-PCR was performed in two technical replicates.

Primer	Primer Sequence (5’ to 3’)
lrrc56 cDNA Exon1F	GGCACAACTCACTCCACTGA
lrrc56 cDNA Exon2R	CAGCGTGTCCTGTCGTGTAT
Beta-actin FW	GACACAGATCATGTTCGAGACC
Beta-actin REV	CCATCACCAGAGTCCATCAC

Table 2.2 Custom Primers for RT-PCR

The program used for the thermal cycler PCR amplification started with an initial denaturation step of 5 minutes at 95°C. Next, the thermal cycler cycled through the following steps 24 times: a 30 second denaturation step at 94°C, a 30 second annealing step at 58°C and a 30 second elongation step at 72°C. The amplification program then ended with a final 5-minute elongation step at 72°C. Afterwards, the PCR reaction was kept at 22^{o}C.

2.10 Overlapping PCR

The coding sequence (CDS) for *lrrc56* was first amplified in two overlapping fragments (893bp and 998bp) from cDNA extracted from 2dpf WT embryos using the primers listed in Table 2.3. 25μL PCR reactions were prepared according to the GoTaq® Green Master Mix (Promega) protocol.

Primer	Primer Sequence (5’ to 3’)
OP FP1 *lrrc56* CDS	AGTTGCAAATGTTGAGTGAAACAGC
OP RP1 *lrrc56* CDS	GGCACTATCTAGATGATTGGAGAGA
OP FP3 *lrrc56* CDS	CTGCCTCTTGATCTAAGAAACTCTC
OP RP3 *lrrc56* CDS	CTTTAATCTGCACTTTCCAGGTG

Table 2.3 Custom Primers for amplifying the *lrrc56* coding sequence.

The program used for the thermal cycler PCR amplification started with an initial denaturation step of 5 minutes at 95°C. Next, the thermal cycler cycled through the following steps 29 times: a 1-minute denaturation step at 94°C, a 1-minute annealing step at 59°C and a 1-minute elongation step at 72°C. The amplification program then ended with a final 10-minute elongation step at 72°C. Afterwards, the PCR reaction was kept at 22°C. Next, using an overlapping PCR with the OP FP1 *lrrc56* CDS and OP RP3 *lrrc56* CDS primers, the 893bp and 998bp fragments were merged to obtain the full CDS of the zebrafish *lrrc56* gene. For the overlapping PCR, a 25µL PCR reaction was prepared using a modified GoTaq® Green Master Mix (Promega) protocol with the two fragments of the *lrrc56* CDS as the DNA templates. Initially the primers, OP FP1 *lrrc56* CDS and OP RP3 *lrrc56* CDS, were not added to the 25µL reaction mix. Instead, in a thermal cycler, the reaction mix was subjected to an initial denaturation step of 5 minutes at 95°C, a 1-minute denaturation step at 94°C, a 1-minute annealing step at 50°C to allow the fragments to anneal at their region of overlap and a 10-minute elongation step at 72°C to allow the addition of nucleotides by GoTaq polymerase to the newly formed amplicons. Afterwards, primers were added to the reaction mix and then the thermal cycler was cycled through the following steps 29 times: a 1-minute denaturation step at 94°C, a 1-minute annealing step at 50°C and a 1-minute elongation step at 72°C. The amplification program then ended with a final 10-minute elongation step at 72°C and the overlapping PCR reaction was then stored at 22°C.

2.11 Cloning / Site-Directed Mutagenesis (SDM)

The overlapping PCR amplicon described in section 2.10 and a poly-A sequence (PA) obtained from the pCS2+ vector were cloned into a p-Drive vector (Qiagen) with the BamHI, HindIII and KpnI restriction sites following the standard cloning procedures of Sambrook & Russell (2001).

To create a zebrafish *lrrc56* mRNA variant possessing the same missense mutation that led to a leucine to proline aa substitution in the Lrrc56 proteins of the 2 autopsied fetuses, SDM was performed on the pDrive vector containing the PA and the *lrrc56* CDS using the Q5® Site Directed Mutagenesis Kit (New England Biolabs) with the primers (Q5SDM_R 5'-GCAGGAAGTCCTTCCAGA-3', Q5SDM_F 5'-TCTTTCTTCCCCGAAGGAGCTGTATGTG-3'), T_m = 62°C. The successful creation of the variant was confirmed by DNA sequencing at OHRI.

2.12 Preparation of capped mRNA

Capped mRNA for the rescue experiments were prepared from using CDS plasmid templates listed in Table 2.4. 10µg of the cDNA plasmid template was linearized using enzymatic digestion with the proper restriction endonuclease for 2 hours at 37°C. The linearized plasmid was then purified using a GE Healthcare Illustra™ purification kit. 1µg of the linearized and purified plasmids were then used as the DNA template with the mMESSAGE mMACHINE Kit (Ambion) and the appropriate RNA polymerase to create capped mRNA.

Plasmid Template	Vector	Restriction Enzyme	RNA Polymerase
lrrc56 CDS	pDrive	Acc65i	SP6
lrrc56 CDS with SDM	pDrive	Acc65i	SP6
eGFP	pCS2+	NotI	SP6

Table 2.4 Plasmid templates for making capped mRNA

2.13 Microinjection of zebrafish embryos

Zebrafish were collected and placed in a petri dish that contained solidified 1% agarose with indented rows to prevent the embryos from moving during the injection process. 50 picograms of

Capped mRNAs (final concentration of 50ng/µl) mixed with RNAse free water and 0.5% phenol red were injected into one cell-stage zebrafish embryos.

3.0 Results

3.1 Expression of *lrrc56* during development

in situ hybridization (ISH) using an anti-sense *lrrc56* probe was used to analyze the expression of the zebrafish *lrrc56* gene during embryogenesis and early larval stages; 7 embryos/larvae were used for each stage. At 12hpf, *lrrc56* was widely expressed in all tissues, including the dorsal forerunner cells forming the Kupffer's vesicle (KV) (Fig. 12A). With the sense *lrrc56* probe which was used as a negative control, we did not observe any staining at 16hpf (Fig.12B). On the other hand, using the anti-sense *lrrc56* probe, expression of *lrrc56* was observed in the head, the pronephric duct primordium, and the neural tube (Fig. 12C). At 24 hpf, expression was observed in the pronephric duct, neural tube, otic vesicle and olfactory pit (Fig. 12D) and at 48 hpf, diffuse expression in the head region was observed (Fig. 12E). While there was some faint expression in the trunk, it is difficult to say if this is true staining or just background. Thus, *lrrc56* is expressed in tissues with motile cilia such as the neural tube that later forms the spinal canal and the KV throughout zebrafish development.

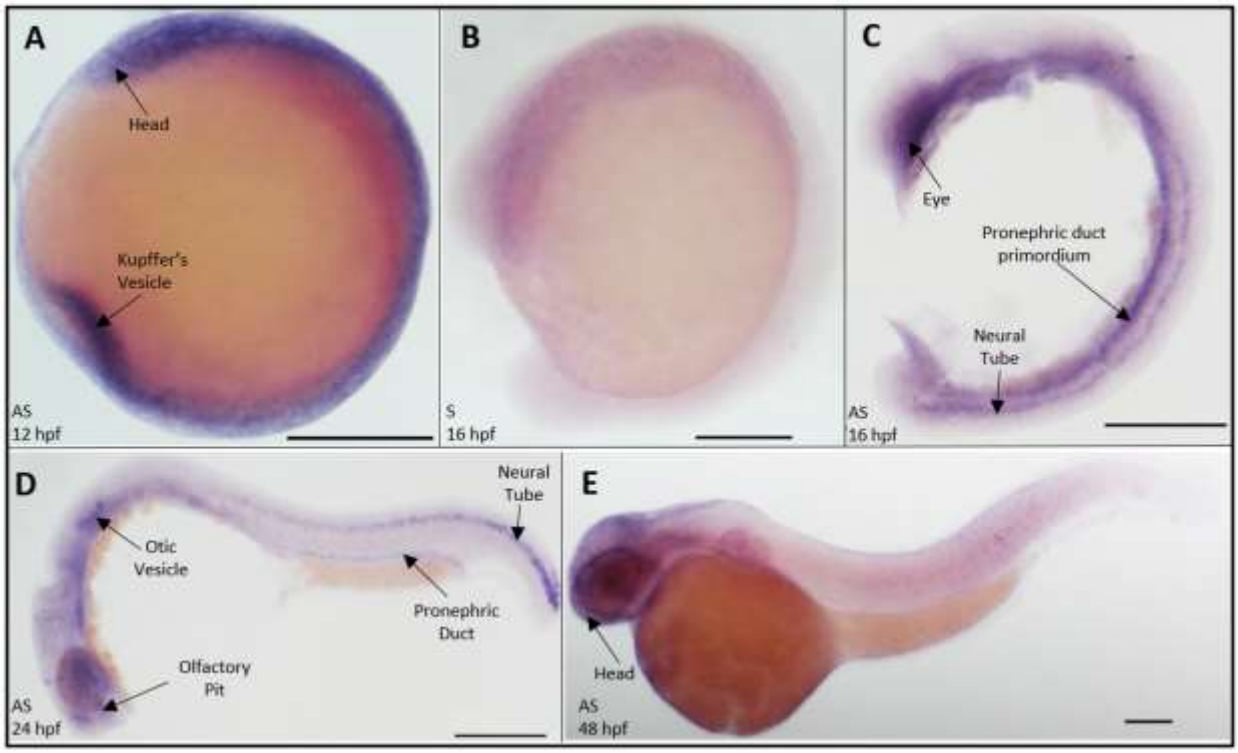

Fig. 1. Whole mount ISH using *lrrc56* probes to analyze the expression of the *lrrc56* gene in WT zebrafish during embryogenesis and early larval stages. Whole-mount ISH on zebrafish embryos obtained from a cross between two WT zebrafish shows A, with an anti-sense *lrrc56* probe, widespread expression at 12 hpf including the dorsal forerunner cells forming the Kupffer's vesicle; B, with a sense *lrrc56* probe, no staining at 16 hpf; C, with an anti-sense probe at 16 hpf, expression in the head, the pronephric duct primordium, and the neural tube; D, with an anti-sense probe at 24 hpf, expression in the pronephric duct, neural tube, otic vesicle and olfactory pit; E, with an anti-sense probe at 48 hpf, diffuse expression in the head. S – sense RNA probe; AS – antisense RNA probe. Scale Bar – 0.05mm.

3.2 Creation of *lrrc56* homozygous mutants

3.2.1 CRISPR/Cas9 Modification of the zebrafish lrrc56 gene

Prior to my arrival, a sgRNA was co-injected with a Cas9 protein into ~200 WT zebrafish (F_0) at the one-cell stage to modify their *lrrc56* genes and these zebrafish were then raised to adulthood. Considering that the Cas9 protein requires the PAM sequence to follow immediately downstream of the target site in addition to the fact that to prevent the creation of a partially functional protein, the target site had to be upstream of the coding sequence for Lrrc56, the earliest possible target site for CRISPR/Cas9 genome editing on the *lrrc56* gene was chosen. This target site was in the first exon of the zebrafish *lrrc56* gene.

The F_0 zebrafish were screened for a mutation at the CRISPR/Cas9 target site that could be transferred to their offspring involved by crossing the F_0 with WT zebrafish. DNA prepared from a pool of ten embryos (F_1) obtained from the crosses was sent for sequencing. After screening 70 F_0 zebrafish, we identified a F_0 with a 4bp deletion at the target site and another F_0 with a 4bp insertion (11bp deletion and a 15bp insertion) in the target site (Fig. 13A). These two *lrrc56* alleles were named *lrrc56*^{ot113} and *lrrc56*^{ot114} respectively in accordance to the University of Ottawa designation and Zebrafish Information Network guidelines (ZFIN). The 4bp deletion mutation caused a premature stop codon immediately downstream of the CRISPR/Cas9 target site that caused the Lrrc56 protein to be shortened from 542aa to 48aa while the 4bp insertion mutation caused a premature stop codon at the CRISPR/Cas9 target site that shortened the Lrrc56 Protein from 542aa to 42aa. Furthermore, through *in silico* analysis using the software Expasy Translate (https://web.expasy.org/translate/), we observed that the truncation of the Lrrc56 protein caused by the 4bp insertion and deletion mutations prevented translation of the 5 LRR motifs that allow

Lrrc56 to be involved in protein-protein interactions (Fig. 14). Due to the complete absence of the LRR motifs after translation, *lrrc56*^{ot113} and *lrrc56*^{ot114} are null alleles.

Adult 4bp deletion F_1 heterozygous mutants presented no abnormal phenotypes during development and were able to breed with other zebrafish properly. These heterozygous mutants were identified by PCR with custom primers designed to amplify the region of the target site coupled with a heteroduplex formation assay (HFA) of the resulting PCR amplicons (Fig. 13B-C). The principle behind HFA is that during the preparation of the assay, mismatches between two strands of a DNA duplex will create a heteroduplex that can be resolved from a normal homoduplex where there is no mismatch by electrophoresis on a poly-acrylamide gel (PAGE). A mismatch that causes a heteroduplex formation resolves as two extra bands on a PAGE gel and the heteroduplex resolves on a PAGE gel slower than a homoduplex. Furthermore, in heterozygous mutants, heteroduplex formation occurs in amounts approximately equal to the amount of homoduplexes.

Preliminary analyses on embryos obtained from crossing the F_1 zebrafish showed that mutants homozygous for the *lrrc56*^{ot113} and *lrrc56*^{ot114} alleles possessed similar phenotypes (Fig. S1). Therefore, we decided to further analyze the phenotypes using the *lrrc56*^{ot113} allele (4bp deletion mutants).

Afterwards, adult heterozygous F_1 adult 4bp deletion zebrafish were crossed with each other and the embryos (F_2) obtained from these crosses were raised to adulthood. The adult homozygous F_2 4bp deletion mutants were then identified by DNA sequencing (Fig. 13D-E) and are referred to as *lrrc56*$^{-/-}$ zebrafish onwards; because these mutants possess two null *lrrc56* alleles, they are *lrrc56* gene knockouts.

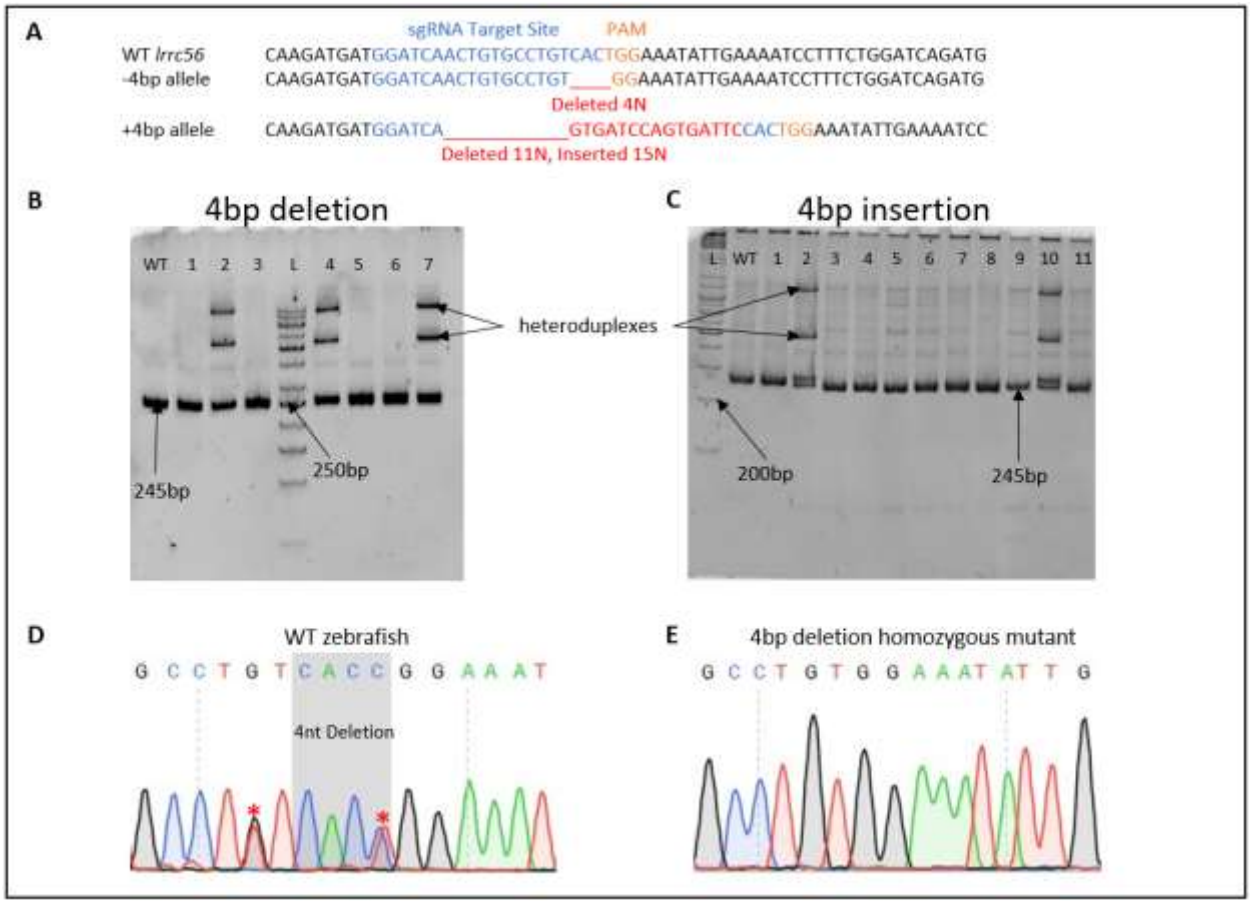

Fig. 13. Gene Analysis of lrrc56 homozygous mutants. A, Sequence for targeting the *lrrc56* gene and resulting insertions and deletions [indels] (alleles *lrrc56*^{ot113}, *lrrc56*^{ot114}). Allele-specific PCR primers were used to identify the *lrrc56* indels (see Materials & Methods). (B-C), Heteroduplex formation assays on a 12% PAGE gel using genomic DNA extracted and amplified by PCR (245bp) from WT control zebrafish and randomly selected F_1 adult zebrafish. The presence of a heteroduplex on the PAGE gel indicates the presence of a WT and mutant allele of the *lrrc56* gene in the zebrafish. L, 50bp DNA ladder (B); 100bp DNA ladder (C); Numbers represent individual zebrafish selected for HFA screening. (D-E), Sequencing chromatograms from F_3 generation larvae show the WT and homozygous 4bp deletion mutants. Red asterisks indicate two previously identified single nucleotide polymorphisms (SNPs) in the WT *lrrc56* gene.

Fig. 14. *in silico* analysis of the Lrrc56 protein in WT zebrafish and *lrrc56* mutants with the alleles *lrrc56*^{ot113} and *lrrc56*^{ot114} using Expasy Translate. aa sequences highlighted in yellow represent sequences that form the 5 LRR motifs found in the zebrafish *lrrc56* gene. The gaps found in the translation of the mRNA sequences from the 4bp deletion and insertion zebrafish mutants indicate the presence of premature stop codons.

3.2.2 *lrrc56*$^{-/-}$ mutants possess a mutant mRNA transcript

After creating zebrafish homozygous for a 4bp deletion in the first exon of their *lrrc56* gene with the CRISPR/Cas9 technology, using a reverse transcriptase PCR (RT-PCR) analysis, we observed that the mutant *lrrc56* mRNA was still transcribed in the *lrrc56*$^{-/-}$ zebrafish (Fig. 15). Furthermore, we observed that the total *lrrc56* mRNA present in the *lrrc56*$^{-/-}$ mutants showed a more intense band after electrophoresis on a 2% agarose gel than the *lrrc56* mRNA in WT zebrafish. One explanation for this is that the WT genomic DNA contamination of the WT *lrrc56* cDNA evidenced by the presence of the 376bp band on the gel could be preventing the proper amplification of the WT cDNA an example of which is seen in Jaakola et al., 2004.

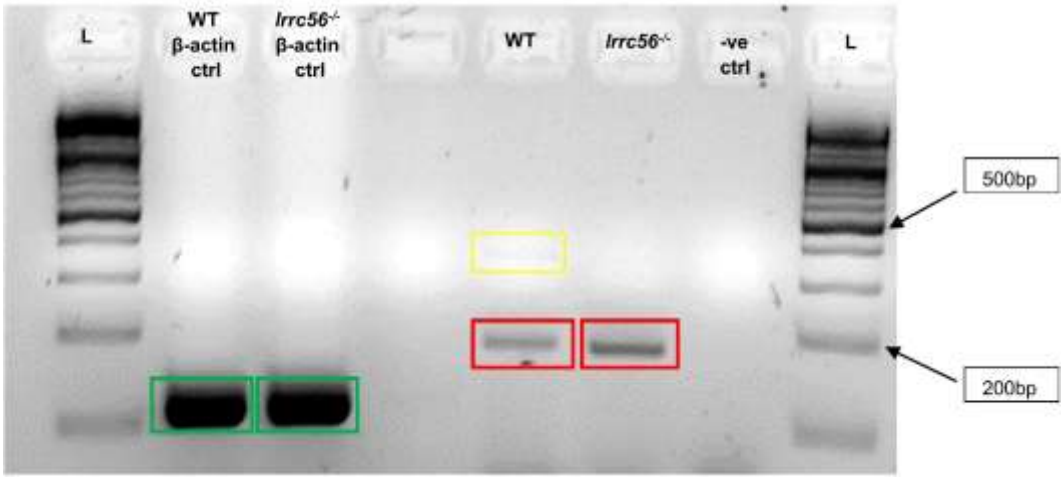

Fig. 15. RT-PCR analysis of *lrrc56* mRNA in WT zebrafish and *lrrc56*$^{-/-}$ mutants. L, 100bp DNA ladder. The bands highlighted with the green boxes represent the β-actin housekeeping gene RT-PCR amplicons for both WT and *lrrc56*$^{-/-}$ corresponding to a size of 116bp. The bands highlighted with the red boxes represent the *lrrc56* gene RT-PCR amplicons for both WT and *lrrc56*$^{-/-}$ corresponding to a size of 197bp. The band highlighted with the yellow box represents genomic DNA in the WT RT-PCR amplicon corresponding to a size of 376bp. The bands were visualized on a 2% agarose gel. Nuclease-Free water was used as the negative control.

3.3 *lrrc56*$^{-/-}$ mutant embryos at 2 dpf show curvatures of the spine

As previously mentioned, heterozygous 4bp deletion mutants presented no abnormal phenotypes. Therefore, after creating homozygous *lrrc56* knockout mutants, we wanted to identify and observe any obvious morphological defects that occurred during development. Grimes et al., 2016 reported that cilia driven cerebrospinal fluid flow was necessary for the proper development of the zebrafish spine. At 2dpf, *lrrc56*$^{-/-}$mutants presented with spine curvatures of varying degrees (Fig. 16B-D). We then classified spinal cord curvature defects relative to the location of the urogenital pore (Fig. 16A red arrow). Curvatures on or before the urogenital pore were classified as severe curvatures (Fig. 16C-D) while curvatures occurring after the urogenital pore were classified as mild curvatures (Fig. 10B arrow). 99% of *lrrc56*$^{-/-}$ mutant embryos (total n=134) possessed spinal defects, with 75% of them possessing mild defects and 24% of them possessing severe defects. On the other hand, just 4.8% and 1.4% of WT embryos had mild and severe spinal defects, respectively, with 93.8 % having a normal spine (total n=146). The presence of these spine defects in *lrrc56*$^{-/-}$ embryos suggests that the proper cerebrospinal fluid flow in the spines of these embryos may be disrupted. Furthermore, we observed that at 2 weeks post fertilization, 61% of *lrrc56*$^{-/-}$ mutants with severe spine curvatures (n=30) died compared to 10% for *lrrc56*$^{-/-}$ mutants with mild spine curvatures (n=30) and 10% for WT zebrafish. Other than the presence of spine curvatures in the *lrrc56*$^{-/-}$ mutants, these mutants showed no other obvious defects during their development.

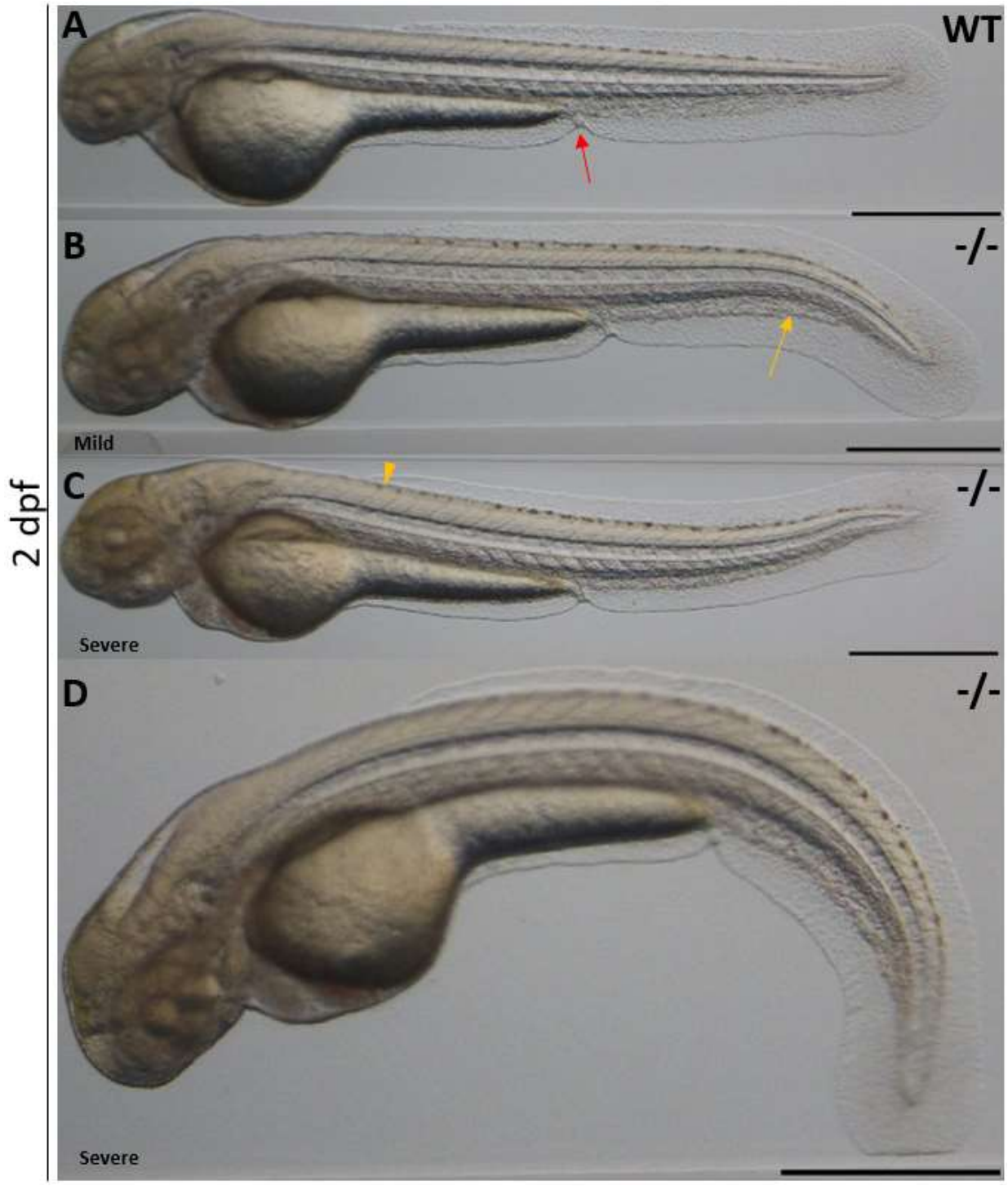
2 dpf
A
WT
B
-/-
Mild
C
-/-
Severe
D
-/-
Severe

Fig. 16. Analysis of spine defects in *lrrc56*$^{-/-}$ mutants. (A-D), Morphology of the spine in zebrafish embryo at 2dpf. A; WT larva, B; *lrrc56*$^{-/-}$ embryos showing a mild spinal defect; (C-D), *lrrc56*$^{-/-}$ larvae with severe spinal defects. Using the location of the urogenital pore (red arrow), defects were classified as mild if they occurred after the urogenital pore – yellow arrow in B, and severe if the defects occurred on or before the urogenital pore – yellow arrowhead in C. Scale bars – 0.5mm.

3.4 *lrrc56*$^{-/-}$ juvenile mutants at 21 dpf show spinal curvatures

After observing curvatures of the spine at 2dpf in *lrrc56*$^{-/-}$ zebrafish, we stained bone and cartilage in these mutant fish, staged at 21dpf, using alizarin red and alcian blue to visualize any bone or cartilage defects, respectively. We staged zebrafish at 21 dpf to ensure that the process of endochondral ossification in the vertebrae had been completed. We observed that the spines of the *lrrc56*$^{-/-}$ zebrafish identified with a severe spinal defect at 2 dpf remained curved even at much later stages of development (n=5) (Fig. 17C). In addition, we noticed that the spacing between vertebrae in the spines of the *lrrc56*$^{-/-}$ mutants was disrupted (Fig. 17B-C, yellow arrowheads). Compared to the WT control (n=5) where spacing was observed between all vertebrae (Fig. 17A red stars), *lrrc56*$^{-/-}$ mutants with a severe curvature of the spine (n=5) had no spacing (Fig. 17C yellow arrowheads) between their vertebrae while mutants with a mild curvature (n=5) had vertebrae with no spacing (Fig. 17B yellow arrowheads) coupled with some vertebrae possessing space between each other (Fig. 17B red stars).

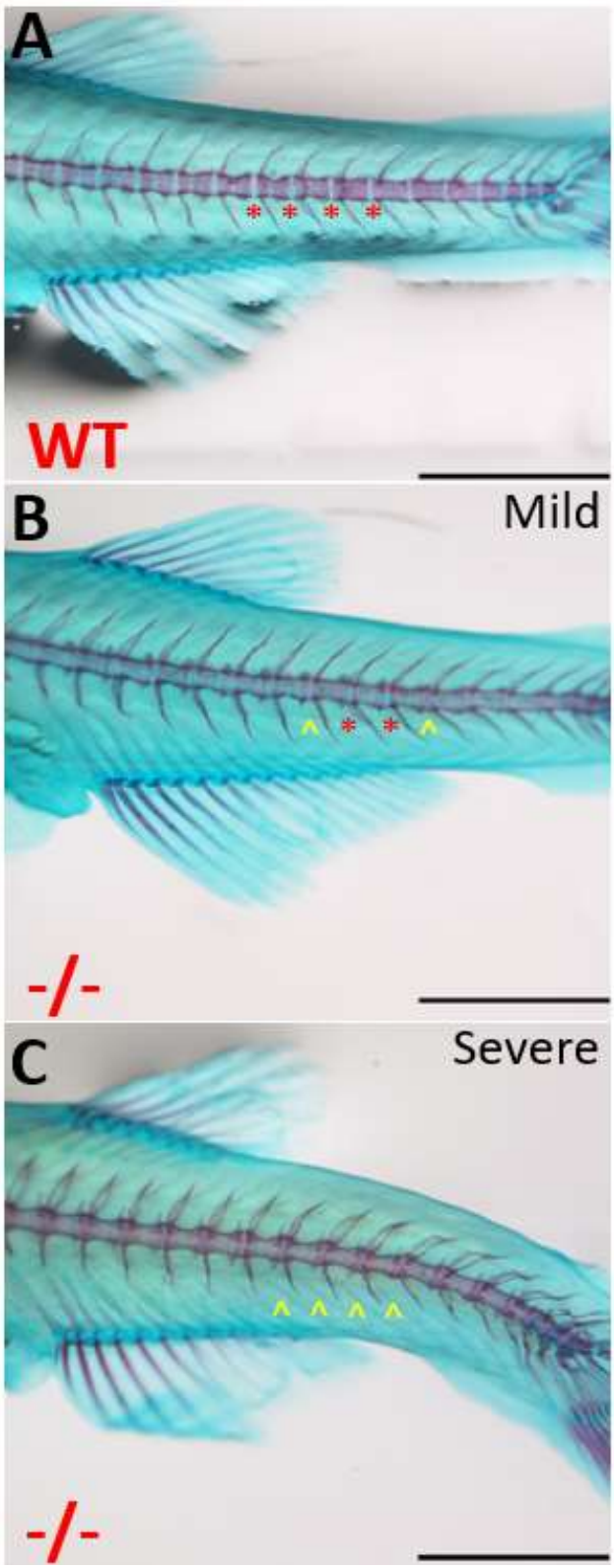

Fig. 17. Bone and Cartilage staining of WT and lrrc56$^{-/-}$ zebrafish at 21 dpf. Zebrafish at 21 dpf were stained with alizarin red for bone and alcian blue for cartilage. A, WT zebrafish spine; B, *lrrc56*$^{-/-}$ mild spinal defect zebrafish spine; C, *lrrc56*$^{-/-}$ severe spinal defect zebrafish spine. Yellow arrowheads indicate no space between the vertebrae. Red stars indicate spacing between the vertebrae. Scale bar – 1mm.

3.5 *lrrc56*$^{-/-}$ zebrafish show laterality defects

Since *lrrc56* was expressed in ciliated tissues and we observed spinal defects during the development of *lrrc56*$^{-/-}$ zebrafish embryos, we decided to examine the laterality of visceral organs in these embryos by gene expression analysis via ISH of forkhead box A3 (*foxA3*), a gene that is expressed in the embryonic liver tissue of zebrafish (Gibert et al., 2011) and cardiac myosin light chain 1 (*cmlc1)* which is expressed in the heart. Through the expression pattern of the *foxA3* gene in the liver bud of zebrafish embryos at 48 hpf, we noticed that the normal laterality of organs in *lrrc56*$^{-/-}$ embryos was disrupted. In 95.7% (n=93) of the WT embryos, the liver bud was located on the left side while the pancreatic bud was located along the mid-line (Fig. 18A, Fig. 19A). In 4.3% of WT embryos, abnormal L/R asymmetry was observed: in 2.15% of the embryos, the location of the liver bud was reversed (Fig. 18B, Fig. 19A) while, in another 2.15% of the embryos, the pancreatic bud was displaced to the left in addition to the liver bud being displaced to the right side (Fig. 18C, Fig.19A). In *lrrc56*$^{-/-}$ embryos, left-right visceral organ patterning was randomized with only 45.92% (n=98) of these embryos having their liver bud on the left side. On the other hand, 48.98% of these embryos had their liver bud on the right side and 5.1% had both the pancreatic and liver buds displaced. To determine if these laterality defects affected multiple visceral organs at the same time or randomly, we checked for the laterality of the liver bud and heart looping at the same time at 48 hpf in WT and *lrrc56*$^{-/-}$ embryos using the expression of the *foxA3* gene in the liver and the expression of the *cmlc1* gene in the heart (Fig. 18D-F). We observed that in both WT and *lrrc56*$^{-/-}$ mutants, no embryos possessed a laterality defect that affected just the liver bud or heart looping individually (Fig. 19B). In the 2.94% (n=34) of WT and 44.64% (n=56) of *lrrc56*$^{-/-}$ embryos that possessed asymmetry defects, a laterality defect in the liver bud was always matched by a laterality defect during heart looping (Fig. 18D-E). Furthermore, in the

2.94% (n=34) WT and 8.93% (n=56) *lrrc56*$^{-/-}$embryos where the pancreas was displaced in addition to the liver bud being displaced, there was no heart looping to the right or left. (Fig. 18F). These results indicate that the *lrrc56* gene is indeed required for the development of normal laterality and that the asymmetry defects observed in *lrrc56*$^{-/-}$ embryos affect the heart and the liver at the same time.

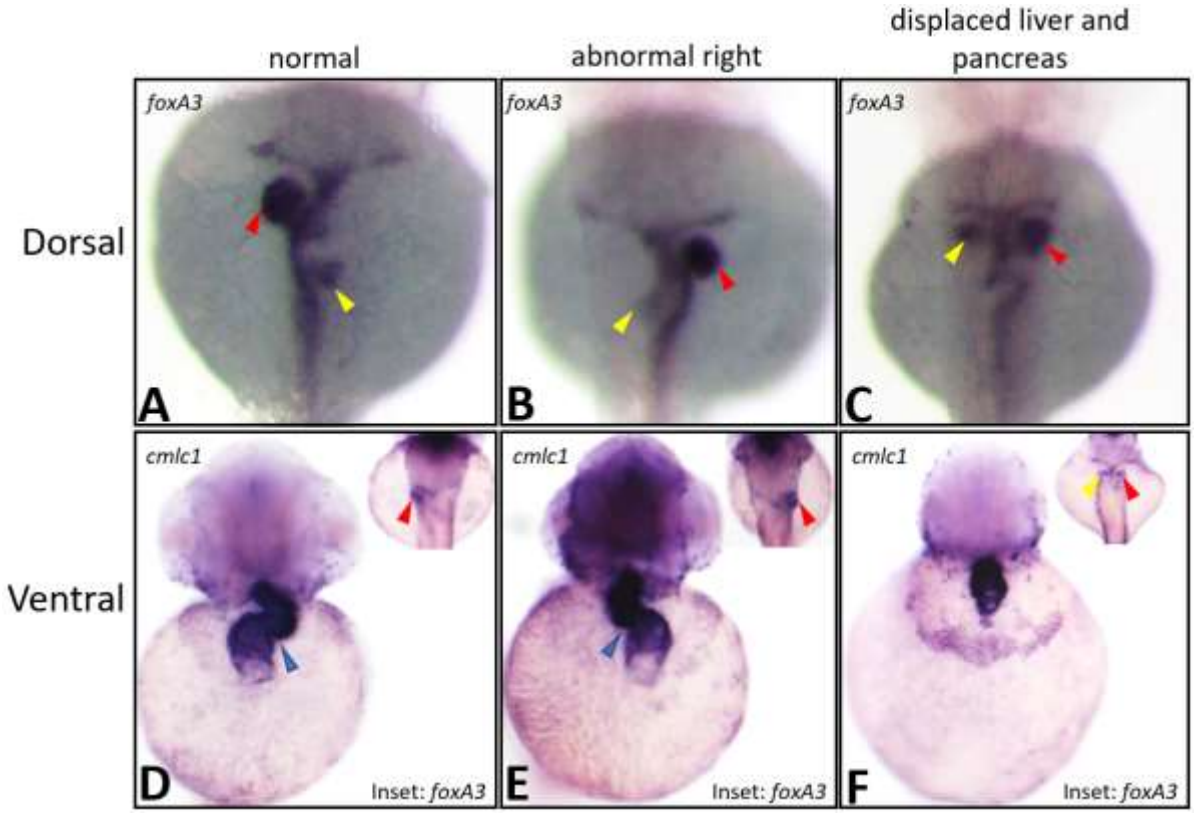

Fig. 18. Expression analysis of *foxA3* and *cmlc1* by ISH in 48 hpf zebrafish embryos. [A-C; inset (D-F)] - dorsal view, D-F ventral view. The expression patterns of *foxA3* in the liver bud (red arrowhead), the pancreatic bud (yellow arrowhead) (A-C) and of *cmlc1* in the heart (blue arrowhead) as observed in WT embryos and *lrrc56*$^{-/-}$ embryos (D-F). Insets in dorsal view show the expression of *foxA3* in the embryos analyzed with *cmlc1*.

A

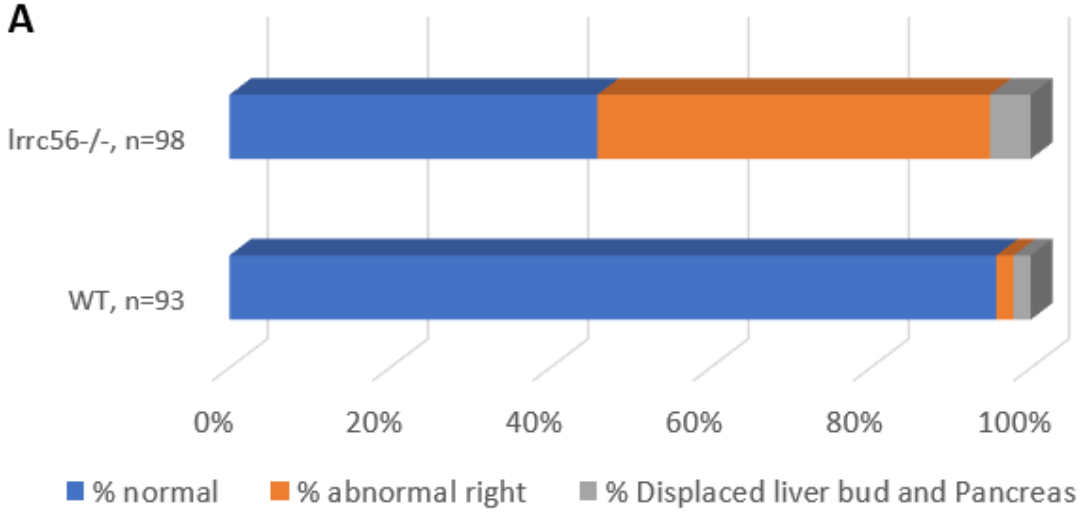

B

cmlc1 + foxa3	Normal	Abnormal Right	Displaced Liver bud + Pancreas	Heterotaxy
WT, n=34	32 (94.12%)	1 (2.94%)	1 (2.94%)	0 (0%)
lrrc56$^{-/-}$, n=56	26 (46.43%)	25 (44.64%)	5 (8.93%)	0 (0%)

Fig. 19. Analysis of L/R asymmetry data for *lrrc56*$^{-/-}$ mutants. A, bar chart showing the percentage of left-right asymmetry of the visceral organs. B, table showing the frequencies of heterotaxy and simultaneous laterality defects of the heart and liver bud in WT and *lrrc56*$^{-/-}$ mutants.

3.6 Cilia are present in the Kupffer's Vesicle (KV) of *lrrc56*$^{-/-}$ zebrafish

To further investigate the observed laterality defects in the zebrafish *lrrc56*$^{-/-}$ embryos at the Left Right Organizer (LRO) – the Kupffer's Vesicle, we performed IHC with an α-tubulin primary antibody to detect cilia in the KV of both WT and *lrrc56*$^{-/-}$ zebrafish. We observed that cilia were still present in the KV of both WT and *lrrc56*$^{-/-}$ embryos at 13hpf (Fig. 20C-D). Measuring these cilia however, revealed that the cilia present in the KV of the *lrrc56*$^{-/-}$ embryos were longer on average than those present in the KV of the WT controls at the same stage. At 13hpf, the average length of a cilium in the KV of the *lrrc56*$^{-/-}$ mutants was 5.22μm while WT cilia in the KV averaged 3.47μm (Fig. 20E).

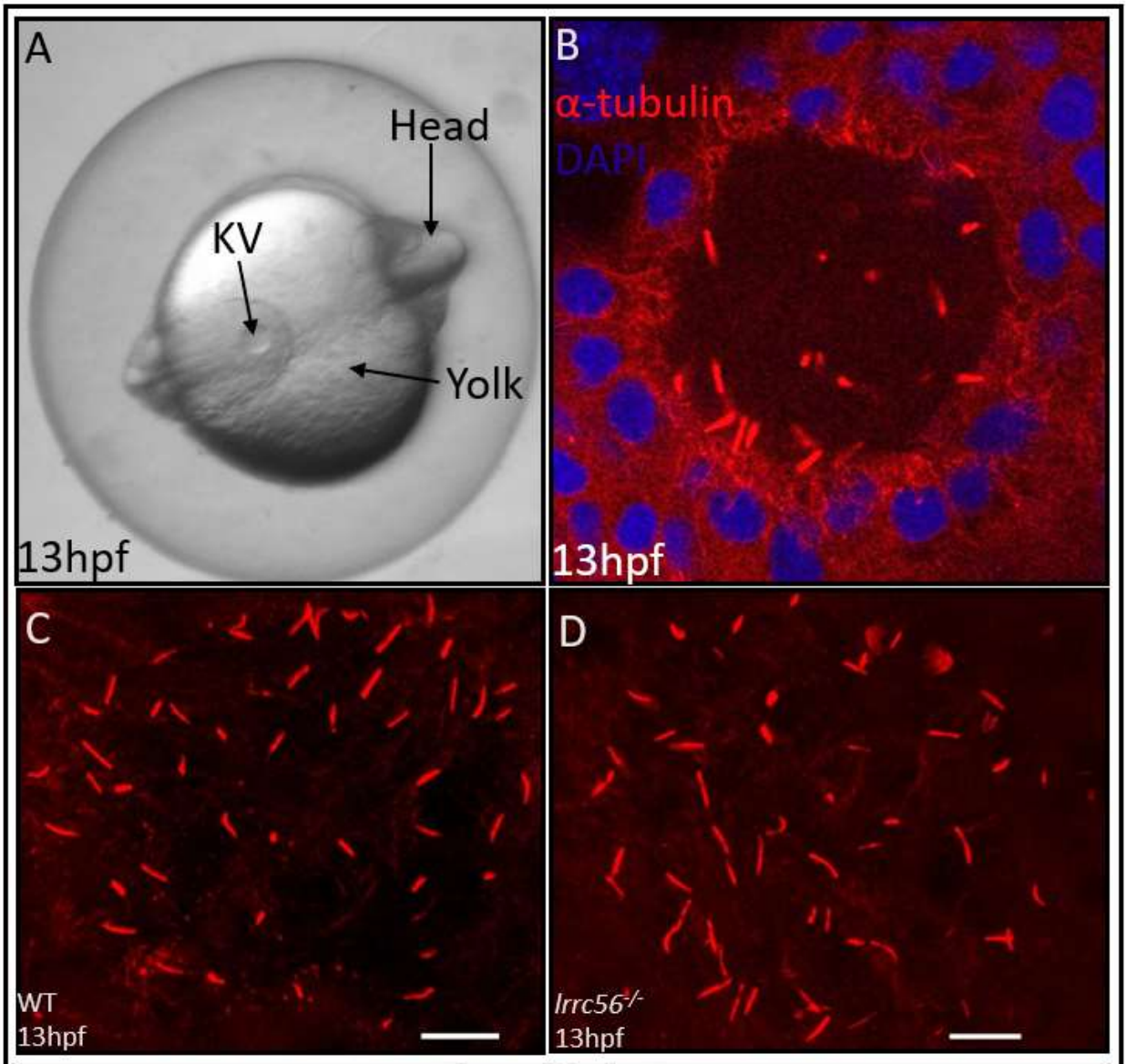

E

	Cilia Length (μm) ± SEM	n
WT	3.47 ± 0.17	43
lrrc56$^{-/-}$	5.22 ± 0.17	43

Fig. 20. Cilia are longer in the KV of *lrrc56*$^{-/-}$ mutants compared to WT zebrafish. IHC on WT and *lrrc56*$^{-/-}$ zebrafish embryos using a α-tubulin antibody. A, Ventral view of a Zebrafish embryo at 13 hpf showing the location of the KV; B, Single Z-stack image of a WT KV showing cilia with DAPI staining the nuclei of the dorsal forerunner cells (DFCs); (C-D), Maximum intensity projection images of cilia in the Kupffer's Vesicle stained with an anti α-tubulin antibody at 13hpf in C, WT and D, *lrrc56*$^{-/-}$ zebrafish. E, at 13 hpf, cilia observed in the KV of *lrrc56*$^{-/-}$ zebrafish are longer than those observed in WT zebrafish; SEM – Standard Error of the Mean. Scale bars - 10μm.

3.7 Laterality Defects in *lrrc56*$^{-/-}$ embryos are rescued with WT *lrrc56* mRNA

To confirm that the laterality and spine defects in the *lrrc56*$^{-/-}$ embryos were due to the 4bp deletion mutation in the *lrrc56* gene, we performed a rescue experiment using 50pg of WT *lrrc56* mRNA. We observed that randomization of asymmetry of the visceral organs still occurred in embryos injected with 50pg eGFP control mRNA (Materials & Methods) as 51.52% (n=66) of the *lrrc56*$^{-/-}$ embryos showed normal placement of the liver bud while 43.94% and 4.95% of these embryos had the liver bud on the right side and both the pancreas and liver bud displaced, respectively (Fig. 21A). On the other hand, 90.41% (n=73) of *lrrc56*$^{-/-}$ embryos injected with the WT *lrrc56* mRNA (Materials & Methods) showed normal placement of the liver bud while only 6.85% and 2.74% of these embryos had the liver bud on the right side and both the pancreas and liver bud displaced, respectively (Fig. 21A). Looking at spinal defects, 75.4% and 23.2% (n=69) of *lrrc56*$^{-/-}$ embryos injected with the eGFP control mRNA presented with mild and severe spinal defects, respectively, with just 1.4% having a normal spine (Fig. 21B). When *lrrc56*$^{-/-}$ mutants were injected with the WT mRNA, 55.8% of these rescued embryos had a normal spine with 37.9% and 6.3% of these embryos possessing mild and severe spinal defects respectively (Fig. 21B) To ascertain that the mutation in one of the LRR active sites of the *lrrc56* gene is the cause of the observed effects in the mutant embryos (Materials & Methods, Fig. 7), we injected *lrrc56*$^{-/-}$ embryos with a *lrrc56* mRNA variant, generated by site-directed mutagenesis (see materials and methods), possessing a leucine to proline amino acid change in the third LRR motif recapitulating what was observed in the human fetuses. Not surprisingly, asymmetry of the liver bud remained randomized with 43.48% (n=23) of these embryos with the liver on the right side, 8.70% having the pancreas displaced in addition to the liver bud and 47.83% with the liver bud on the normal left side. Concerning spinal defects, 100% of these embryos with the mRNA variant possessed spine

curvatures with 51.7% (n=29) possessing mild spinal curvatures and 48.3% possessing severe spinal curvatures (Fig. 21B). The successful rescue of *lrrc56*$^{-/-}$ embryos with WT *lrrc56* mRNA and the unsurprising lack of rescue with the *lrrc56* mRNA variant indicate that the asymmetry defects observed in these embryos are indeed due to the mutation in the *lrrc56* gene and that the mutation in one of the LRR active sites is enough to cause laterality defects. Given that this missense mutation is the same one identified in the human fetuses, it is the likely cause of the asymmetry defects observed in these fetuses.

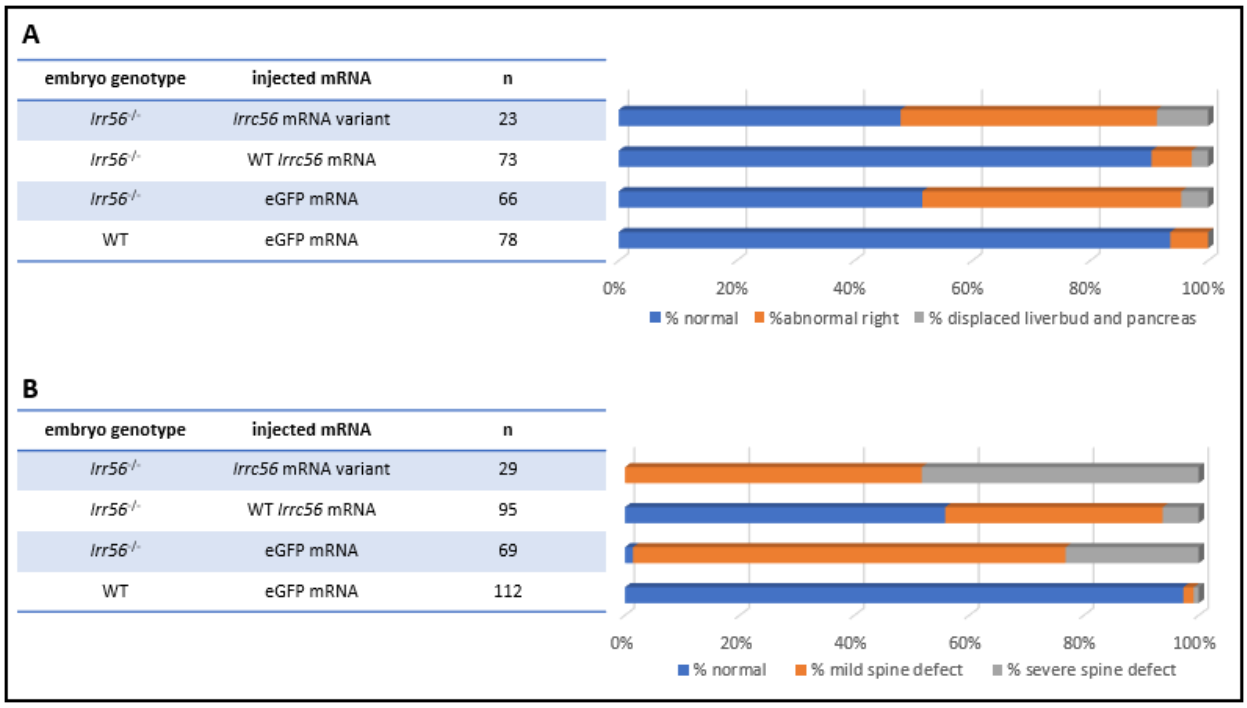

Fig. 21. Analysis of data obtained from the rescue experiment. A, Bar chart showing the left-right asymmetry of the liver bud after rescuing *lrrc56*$^{-/-}$ embryos with WT *lrrc56*$^{-/-}$ mRNA and after injecting a *lrrc56*$^{-/-}$ mRNA Variant (see Materials & Methods) into *lrrc56*$^{-/-}$ embryos. B, Bar chart showing the percentage of *lrrc56*$^{-/-}$ embryos at 48 hpf with spinal defects after rescue with WT *lrrc56*$^{-/-}$ mRNA and after injecting a *lrrc56*$^{-/-}$ mRNA Variant (see Materials & Methods).

4.0 Discussion

4.1 Knocking out the *lrrc56* gene in zebrafish results in Primary Ciliary Dyskinesia (PCD) associated phenotypes

In this study, we created a zebrafish *lrrc56* gene knockout using the CRISPR/Cas9 genome editing technology to model ciliopathy associated symptoms observed in autopsied human fetuses that were linked to a mutation of their *LRRC56* gene. To begin with, we first characterized the development of the spine in our *lrrc56*$^{-/-}$ mutants with the goal of determining if these mutants were displaying zebrafish specific symptoms of a ciliopathy. This is because previous zebrafish models of human ciliopathies have shown that curvatures of the spine are characteristic of a ciliopathy in zebrafish (Duldulao, Lee, & Sun, 2009) and the occurrence of the spine curvatures was reported to be a result of the improper flow of cerebrospinal fluid in the spines of these zebrafish (Grimes et al, 2016). In our *lrrc56*$^{-/-}$ mutants, we observed curvatures of the spine that we then further classified into mild curvatures and severe curvatures based on the location of the curvature relative to the urogenital pore. Coupled with the curvatures of the spine, in some preliminary results, we also observed that the spacing between vertebrae of the *lrrc56*$^{-/-}$ mutants was reduced and the frequency of this reduction was greater in the *lrrc56*$^{-/-}$ mutants with severe curvatures of the spine. As these preliminary data were obtained from a small sample size, these results will need confirmation.

Other than the zebrafish specific spine curvatures, we wanted to characterize the L/R asymmetry of the visceral organs in our *lrrc56*$^{-/-}$ mutants. In this study, we did not determine the molecular onset of laterality defects of the visceral organs in zebrafish embryos but used instead, previously established timepoints where we could observe the visceral organs themselves to determine any laterality defects. As previously mentioned (1.5.1 Cilia and Determination of Asymmetry in

Zebrafish), the liver bud emerges on the left side of the zebrafish larva from a dorsal view by 30 hpf (Grimes & Burdine, 2017) in the WT condition; cardiac jogging in zebrafish, where a leftward 'jog' is observed in the WT condition (Khodiyar, Howe, Talmud, Breckenridge, & Lovering, 2013), can be observed at 24 hpf and cardiac looping where the initially straight embryonic heart tube becomes transformed into a helically wound loop that is normally seen with a counterclockwise winding can be observed beginning at 36hpf (Männer, 2009). We decided to use the heart (cardiac looping) and the liver bud as representative visceral organs in the *lrrc56*$^{-/-}$ mutants because at 2 dpf, the timepoint when we characterize the morphology of the spine in the *lrrc56*$^{-/-}$ mutants, these two organs have well defined asymmetrical locations that are easily observable during the development of the zebrafish embryo. To check for *Situs inversus totalis* in our *lrrc56*$^{-/-}$ embryos, we performed a gene expression analysis on WT and *lrrc56*$^{-/-}$ zebrafish embryos at 48 hpf using the *foxA3* and the *cmlc1* genes simultaneously in zebrafish embryos to identify the visceral locations of the liver bud and the heart respectively. We then observed that *Situs inversus totalis* of these visceral organs occurred in approximately 45% of the *lrrc56*$^{-/-}$ mutants (Fig. 18, 19B).

As previously mentioned in 1.3 Defects of Axonemal Dyneins are associated with Ciliopathies., in humans, *Situs inversus totalis* occurs in 40%-50% of individuals with PCD. This recapitulates what we observed in our zebrafish *lrrc56* knockout model where ~45% of them presenting with *situs inversus totalis* of the liver bud and heart looping. This result obtained using a zebrafish *lrrc56* knockout model provides some evidence that the defects in the *LRRC56* gene of the autopsied fetuses is responsible for the PCD associated phenotypes observed in these fetuses.

To confirm that the curvatures of the spine and the visceral organ asymmetry randomization observed in the *lrrc56*$^{-/-}$ mutant zebrafish were due to knocking out the *lrrc56* gene in the *lrrc56*$^{-/-}$ zebrafish, we attempted to rescue these phenotypes by injecting WT *lrrc56* mRNA into these

embryos. After the injection, we observed that while the laterality defects phenotype was rescued, the curvature of the spine phenotype was partially rescued (Fig. 21). This difference in the totality of the rescue between the two phenotypes could be a result of the amounts of the WT *lrrc56* mRNA injected. During the rescue experiment, we injected 50pg and 100pg of the WT *lrrc56* mRNA into different *lrrc56*$^{-/-}$ embryos and we observed that while the embryos survived with the 50pg injection, the survived poorly with the 100pg injection. While we could not create a zebrafish model with the homozygous missense mutation observed in the autopsied fetuses, we wanted to observe the effects of injecting a *lrrc56* mRNA possessing the missense mutation (Materials & Methods) into the *lrrc56*$^{-/-}$ mutants. Since this missense mutation was suspected to be the cause of the laterality defects in the autopsied fetuses, we expected that the injection of the *lrrc56* mRNA variant would not rescue the randomization of asymmetry or the spinal defects in the *lrrc56*$^{-/-}$ embryos. Not surprisingly, after injection of the variant mRNA, neither the proper L/R asymmetry of the visceral organs nor the normal morphology of the spine was restored during development in the *lrrc56*$^{-/-}$ mutant embryos (Fig. 21). Therefore, we can conclude that the spine and laterality defects observed in the *lrrc56*$^{-/-}$ mutants show that *lrrc56* plays a role in the proper development of cilia and that the missense variant and our knockout both hinder the proper functioning of the *lrrc56* gene.

4.2 No obvious cardiac anomalies were observed in the *lrrc56*$^{-/-}$ zebrafish mutants.

So far, we have reported that the *lrrc56*$^{-/-}$ mutants displayed laterality defects, recapitulating what was observed in the autopsied fetuses but while the two fetuses presented with cardiac anomalies, the knockout mutants in our zebrafish model did not present with any obvious cardiac defects during early development. This absence of heart defects in our *lrrc56*$^{-/-}$ mutants could explain the viability of the *lrrc56*$^{-/-}$ zebrafish mutants and the lack of viability observed in the human fetuses

because the fetal heart is an important component of the circulatory system that is necessary for maintaining nutrition and oxygen delivery to the developing tissues of the fetus (Gleason & Juul, 2017).

Previous research (Harrison, Shapiro, & Kennedy, 2016; Applegate, Goske, Pierce, & Murphy, 1999) indicated that cardiac anomalies occur 50-100% of the time when PCD and heterotaxy co-exist. When we checked for the presence of heterotaxy in our *lrrc56*$^{-/-}$ mutants (Fig. 19B), we observed that while our results for *situs inversus totalis* were similar to those observed in humans with PCD at ~45%, we did not observe any heterotaxy in either the WT or *lrrc56*$^{-/-}$ zebrafish embryos we analyzed. For the WT embryos, the absence of heterotaxia was not surprising because as earlier mentioned, heterotaxia occurs rarely in humans, with an incidence of just 1:10,000 newborn births (Mujo, Finnegan, Joshi, Wilcoxen, & Reed, 2015). However, the incidence of heterotaxia in our *lrr56*$^{-/-}$ mutants did not recapitulate the incidence of heterotaxia in human with PCD since we did not observe heterotaxia in our *lrrc56*$^{-/-}$ mutants while the incidence of heterotaxia in human PCD is at least 12% (Knowles, Zariwala, & Leigh, 2016). Currently not much is known about the causes of heterotaxia vs. *situs inversus totalis* when coupled with PCD. Therefore, we concluded that the absence of heterotaxia in our *lrrc56*$^{-/-}$ mutants could be one possible explanation for the lack of cardiac anomalies in these mutants.

Another possible reason for the absence of cardiac anomalies in the *lrrc56*$^{-/-}$ mutants is that while the zebrafish and mammalian heart share many similarities (Genge et al., 2016), the zebrafish heart possesses a remarkable ability to completely regenerate after injury while the mammalian heart cannot regenerate after injury (Nemtsas, Wettwer, Christ, Weidinger, & Ravens, 2010). This therefore suggests that cardiac anomalies that might have occurred very early during the

development of the *lrrc56*$^{-/-}$ may have been repaired by the time of our analyses, leading us to conclude that there were no obvious heart defects.

Finally, the zebrafish *lrrc56*$^{-/-}$ mutants we created and analyzed possessed a null mutation that prevented the production of the Lrrc56 protein. On the other hand, the two autopsied fetuses possessed a missense LRRC56 mutation which did not prevent the formation of a mutant LRRC56 protein. The presence of this mutant LRRC56 protein might be a factor responsible for the cardiac anomalies observed in these fetuses because the mutant LRRC56 protein might have gained a new function that negatively affects the proper development of the heart in these fetuses. To test this hypothesis in future studies, it will be important to create zebrafish mutants that are homozygous for the missense mutation observed in the human fetuses. This time, instead of using the endogenous non-homologous end joining (NHEJ) CRISPR/Cas9 system to create the knockout model, the missense mutation would be introduced into the zebrafish *lrrc56* gene by a "knock-in", with the use of the homology directed repair (HDR) CRISPR/ Cas9 system (Fig. 11). Alternatively, under the control of the *cmlc1* promoter which activates expression in the heart, transgenic zebrafish in the *lrrc56*$^{-/-}$ background that express the *lrrc56* missense variant could be created to specifically observe the effects of the missense Lrrc56 protein on the proper development of the heart. While we did not observe any obvious cardiac anomalies occurring with the injection of the *lrrc56* mRNA variant into the *lrrc56*$^{-/-}$ zebrafish, it is possible that there were defects that were not immediately obvious or that may have appeared after the stage at which we analyzed the *lrrc56*$^{-/-}$ fish. Therefore, in the future, measurements of the cardiac rate at different stages of development coupled with analyses of the morphologies of the internal structures of the heart (the atrium and the ventricle), would provide more detailed information on the presence or absence of cardiac defects in the *lrrc56*$^{-/-}$ mutants (De Luca et al., 2014; Genge et al., 2016).

4.3 *lrrc56*$^{-/-}$ mutants possess elongated cilia during KV organogenesis

To better understand the cause of the displayed laterality defects, we looked at the cilia in the KV at 13 hpf and observed that while they were present in the KV of *lrrc56*$^{-/-}$ zebrafish, they were longer than in WT controls. Currently, there is a lack of consensus regarding cilia lengths in the KV of WT zebrafish at 13 hpf with values ranging from 2.6µm to 7µm (Gokey, Ji, Tay, Litts, & Amack, 2015); However, in our experiments the lengths of cilia in our WT controls average 3.47µm which is similar to the average WT cilia length reported in Gao, Wang, Amack, & Mitchell, 2010 at 3.5 µm. While Bonnefoy et al., 2018 reported severely dyskinetic cilia in *Trypanosoma brucei* cell lines possessing pLeu140pro, the missense mutation observed in the *LRRC56* gene of the autopsied fetuses, we have not yet identified how these elongated cilia in the *lrrc56*$^{-/-}$ mutants will affect fluid flow in the KV. In the future, we will first test the fluid movement generated by these elongated cilia in the KV of the *lrrc56*$^{-/-}$ mutants. This cilia-driven fluid flow in the KV can be observed following the injection of fluorescent microbeads into the lumen of the KV while using a high-speed fluorescent microscope to capture the movement of the microbeads (Wang, Yost, & Amack, 2013). Other than the cilia in the KV, in the future, the length of cilia found in other organs such as in the spinal canal, the lateral lines, the pronephric ducts and the otic vesicle can also be measured using IHC with an α-tubulin antibody coupled with fluorescent confocal microscopy. The length data obtained from the IHC would allow us to identify if cilia are also elongated in ciliated organs other than the KV.

4.4 *lrrc56* may be involved in terminating the growth of motile cilia

Bonnefoy et al., 2018 reported an absence of outer dynein arms restricted to the distal portion of the axoneme in *Trypanosoma brucei* cell lines possessing either *LRRC56* null mutations or the pLeu140pro mutation. So far, we have no data to support this finding. Therefore, in the future,

transmission electron microscopy on cilia extracted from the spines and KVs of *lrrc56*$^{-/-}$ mutants would provide evidence on the presence/absence of ODAs on the axonemes of these cilia.

As mentioned in the introduction, previous studies have proposed a model in which LRRC56 associates with inter-flagellar transport (IFT) trains as a cargo adaptor to transport ODAs from the cytoplasm to the cilia compartment where the ODAs are then released to bind to the ODA docking complex (ODA-DC) on the axoneme (Fig. 6; Bonnefoy et al., 2018; Desai et al., 2015; Dean & Mitchell, 2015). These IFT complexes have previously been proposed as the main regulators of cilia growth in ciliated cells (Keeling, Tsiokas, & Maskey, 2016). In fact, previous studies using *Chlamydomonas reinhardtii* have shown that the increased accumulation or activity of the anterograde IFT complex leads to further elongation of the cilia, whereas a decrease in the mobility of this anterograde complex leads to the generation of shorter cilia (Marshall & Rosenbaum, 2001; Marshall, Qin, Brenni, & Rosenbaum, 2005). Based on our observations of elongated cilia in the KV of *lrrc56*$^{-/-}$ mutants, it is possible that the association of Lrrc56 with the IFT complex during the anterograde transport of the ODA complexes from the cytoplasm to the ciliary compartment slows down the velocity of the anterograde IFT complex. Therefore, in the *lrrc56*$^{-/-}$ mutants where the Lrrc56 protein is absent, the anterograde IFT complex now gains increased mobility. Since Lrrc56 disassociates from the IFT complex after delivering the mature ODA complexes to the axonemal docking sites, it is not likely that retrograde IFT is affected in the *lrrc56*$^{-/-}$ mutants. To test this theory, IFT88, an important component of the IFT complex, can be tagged with a fluorophore that would allow the visualization of the IFT during anterograde and retrograde transport in WT and *lrrc56*$^{-/-}$ zebrafish. Afterwards, time-lapse image sequences which are then assembled into kymographs can be used to determine the velocities of the IFT complexes during retrograde and anterograde transport (Besschetnova et al., 2010) in the cilia of the WT and lrrc56^{-}

$^{-/-}$ zebrafish. Furthermore, if indeed the mobility of the anterograde IFT is increased while the mobility of retrograde IFT remains unaffected in the elongated cilia possessed by the *lrrc56*$^{-/-}$ mutants, it is expected that there would be greater fluorescence at the tips of these elongated cilia, indicative of an accumulation of IFT88 due to increased anterograde velocities and unchanged retrograde velocities.

In 2011, Abdul-Majeed, Moloney, & Nauli, 2011 showed that intracellular cyclic adenosine monophosphate (cAMP), cAMP-dependent protein kinase (PKA), mitogen-activated protein kinase (MAPK), protein phosphatase-1 (PP-1), and cofilin regulate non-motile cilia length in vascular endothelial cells. Therefore, in the future, by analyzing the concentrations of these intra cellular proteins in ciliated cells of the *lrrc56*$^{-/-}$ mutants, we can determine if these intracellular proteins are affected by knocking out the *lrrc56* gene and if the regulation of motile cilia length recapitulates or contrasts from the regulation of non-motile cilia length.

5.0 Conclusion

LRRC56 is the newest addition to the family of proteins including *DNAI1*, *DNAH5*, *DNAI2* and even *LRR* proteins like *LRRC50* and *LRRC6* (Damseh, Quercia, Rumman, Dell, & Kim, 2017) that are responsible for the proper development of the outer dynein arms during cilia growth. Using zebrafish as a model, we provide direct evidence that knocking out *lrrc56* and the introduction of a missense mutation in one of the LRR functional sites (Fig. 7) leads to ciliopathy associated symptoms descriptive of PCD. Our results indicate that the physical anomalies observed in the autopsied human fetuses are a result of the homozygous missense variant of their respective *LRRC56* gene.

References

Abdul-Majeed, S., Moloney, B. C., & Nauli, S. M. (2011). Mechanisms regulating cilia growth and cilia function in endothelial cells. *Cellular and Molecular Life Sciences*, *69*(1), 165-173. https://doi.org/10.1007/s00018-011-0744-0

Afzelius, B. (1959). Electron microscopy of the sperm tail results obtained with a new fixative. *The Journal of Cell Biology*, *5*(2), 269-278. https://doi.org/10.1083/jcb.5.2.269

Ahmed, N. T., Gao, C., Lucker, B. F., Cole, D. G., & Mitchell, D. R. (2008). Oda16 aids axonemal outer row dynein assembly through an interaction with the intraflagellar transport machinery. *The Journal of Cell Biology*, *183*(2), 313-322. https://doi.org/10.1083/jcb.200802025

Applegate, K. E., Goske, M. J., Pierce, G., & Murphy, D. (1999). Situs revisited: imaging of the heterotaxy syndrome. *RadioGraphics*, *19*(4), 837-852. https://doi.org/10.1148/radiographics.19.4.g99jl31837

Austin-Tse, C., Halbritter, J., Zariwala, M., Gilberti, R., Gee, H., Hellman, N., & Hildebrandt, F. (2013). Zebrafish ciliopathy screen plus human mutational analysis identifies c21orf59 and ccdc65 defects as causing primary ciliary dyskinesia. *The American Journal of Human Genetics*, *93*(4), 672-686. https://doi.org/10.1016/j.ajhg.2013.08.015

Babu, D., & Roy, S. (2013). Left-right asymmetry: cilia stir up new surprises in the node. *Open Biology*, *3*(5), 130052-130052. https://doi.org/10.1098/rsob.130052

Baker, K., Holtzman, N. G., & Burdine, R. D. (2008). Direct and indirect roles for nodal signaling in two axis conversions during asymmetric morphogenesis of the zebrafish heart. *Proceedings of the National Academy of Sciences*, *105*(37), 13924-13929. https://doi.org/10.1073/pnas.0802159105

Berbari, N. F., O'Connor, A. K., Haycraft, C. J., & Yoder, B. K. (2009). The primary cilium as a complex signaling center. *Current Biology*, *19*(13), R526-R535. https://doi.org/10.1016/j.cub.2009.05.025

Besschetnova, T. Y., Kolpakova-Hart, E., Guan, Y., Zhou, J., Olsen, B. R., & Shah, J. V. (2010). Identification of signaling pathways regulating primary cilium length and flow-mediated adaptation. *Current Biology*, *20*(2), 182-187. https://doi.org/10.1016/j.cub.2009.11.072

Boehlke, C., Janusch, H., Hamann, C., Powelske, C., Mergen, M., Herbst, H., & Kuehn, E. W. (2015). A cilia independent role of ift88/polaris during cell migration. *PLOS ONE*, *10*(10), e0140378. https://doi.org/10.1371/journal.pone.0140378

Bonnefoy, S., Watson, C., Kernohan, K., Lemos, M., Hutchinson, S., & Poulter, J. (2018). Biallelic mutations in lrr56 encoding a protein associated with intraflagellar transport, cause mucociliary clearance and laterality defects. *American Journal of Human Genetics*, *103*(5), 727-739. https://doi.org/10.1101/288852

Brummett, A. R., & Dumont, J. N. (1978). Kupffer's vesicle in fundulus heteroclitus: A scanning and transmission electron microscope study. *Tissue and Cell*, *10*(1), 11-22. https://doi.org/10.1016/0040-8166(78)90003-4

Burgess, S. A., Walker, M. L., Sakakibara, H., Knight, P. J., & Oiwa, K. (2003). Dynein structure and power stroke. *Nature*, *421*(6924), 715-718. https://doi.org/10.1038/nature01377

Cherkas, V., Grebenyuk, S., Osypenko, D., Dovgan, A. V., Grushevskyi, E. O., Yedutenko, M., & Belan, P. (2018). Measurement of intracellular concentration of fluorescently-labeled targets in living cells. *PLOS ONE*, *13*(4), e0194031. https://doi.org/10.1371/journal.pone.0194031

Christensen, S. T., Pedersen, L. B., Schneider, L., & Satir, P. (2006). Sensory cilia and integration of signal transduction in human health and disease. *Traffic*, *8*(2), 97-109. https://doi.org/10.1111/j.1600-0854.2006.00516.x

Cong, L., Ran, F. A., Cox, D., Lin, S., Barretto, R., Habib, N., & Zhang, F. (2013). Multiplex genome engineering using crispr/cas systems. *Science*, *339*(6121), 819-823. https://doi.org/10.1126/science.1231143

Damseh, N., Quercia, N., Rumman, N., Dell, S. D., & Kim, R. H. (2017). Primary ciliary dyskinesia: mechanisms and management. *The Application of Clinical Genetics*, *10*, 67-74. https://doi.org/10.2147/TACG.S127129

De Luca, E., Zaccaria, G. M., Hadhoud, M., Rizzo, G., Ponzini, R., Morbiducci, U., & Santoro, M. M. (2014). Zebrabeat: a flexible platform for the analysis of the cardiac rate in zebrafish embryos. *Scientific Reports*, *4*(1). https://doi.org/10.1038/srep04898

Dean, A. B., & Mitchell, D. R. (2015). Late steps in cytoplasmic maturation of assembly-competent axonemal outer arm dynein in chlamydomonas require interaction of oda5 and oda10 in a complex. *Molecular Biology of the Cell*, *26*(20), 3596-3605. https://doi.org/10.1091/mbc.e15-05-0317

Deltcheva, E., Chylinski, K., Sharma, C. M., Gonzales, K., Chao, Y., Pirzada, Z. A., & Charpentier, E. (2011). Crispr rna maturation by trans-encoded small rna and host factor rnaseiii. *Nature*, *471*(7340), 602-607. https://doi.org/10.1038/nature09886

Deneka, D., Sawicka, M., Lam, A. K., Paulino, C., & Dutzler, R. (2018). Structure of a volume-regulated anion channel of the lrrc8 family. *Nature*, *558*(7709), 254-259. https://doi.org/10.1038/s41586-018-0134-y

Desai, P. B., Freshour, J. R., & Mitchell, D. R. (2015). Chlamydomonasaxonemal dynein assembly locus oda8 encodes a conserved flagellar protein needed for cytoplasmic maturation of outer dynein arm complexes. *Cytoskeleton*, *72*(1), 16-28. https://doi.org/10.1002/cm.21206

Desgrange, A., Le Garrec, J., & Meilhac, S. M. (2018). Left-right asymmetry in heart development and disease: forming the right loop. *Development*, *145*(22), dev162776. https://doi.org/10.1242/dev.162776

Duldulao, N. A., Lee, S., & Sun, Z. (2009). Cilia localization is essential for in vivo functions of the joubert syndrome protein arl13b/scorpion. *Development*, *136*(23), 4033-4042. https://doi.org/10.1242/dev.036350

Dutcher, S. K. (1995). Flagellar assembly in two hundred and fifty easy-to-follow steps. *Trends in Genetics*, *11*(10), 398-404. https://doi.org/10.1016/s0168-9525(00)89123-4

Essner, J. J. (2005). Kupffer's vesicle is a ciliated organ of asymmetry in the zebrafish embryo that initiates left-right development of the brain, heart and gut. *Development*, *132*(6), 1247-1260. https://doi.org/10.1242/dev.01663

Essner, J. J., Vogan, K. J., Wagner, M. K., Tabin, C. J., Yost, H. J., & Brueckner, M. (2002). Conserved function for embryonic nodal cilia. *Nature*, *418*(6893), 37-38. https://doi.org/10.1038/418037a

Faubel, R., Westendorf, C., Bodenschatz, E., & Eichele, G. (2016). Cilia-based flow network in the brain ventricles. *Science*, *353*(6295), 176-178. https://doi.org/10.1126/science.aae0450

Fliegauf, M., Benzing, T., & Omran, H. (2007). When cilia go bad: cilia defects and ciliopathies. *Nature Reviews Molecular Cell Biology*, *8*(11), 880-893. https://doi.org/10.1038/nrm2278

Gao, C., Wang, G., Amack, J. D., & Mitchell, D. R. (2010). Oda16/wdr69 is essential for axonemal dynein assembly and ciliary motility during zebrafish embryogenesis. *Developmental Dynamics*, *239*(8), 2190-2197. https://doi.org/10.1002/dvdy.22355

Genge, C. E., Lin, E., Lee, L., Sheng, X., Rayani, K., Gunawan, M., & Tibbits, G. F. (2016). The zebrafish heart as a model of mammalian cardiac function. *Reviews of Physiology, Biochemistry and Pharmacology*, 99-136. https://doi.org/10.1007/112_2016_5

Gibbons, I. R. (1963). Studies on the protein components of cilia from tetrahymena pyriformis. *Proceedings of the National Academy of Sciences*, *50*(5), 1002-1010. https://doi.org/10.1073/pnas.50.5.1002

Gibert, Y., Lattanzi, V. J., Zhen, A. W., Vedder, L., Brunet, F., Faasse, S. A., & Fraenkel, P. G. (2011). Bmp signaling modulates hepcidin expression in zebrafish embryos independent of hemojuvelin. *PLoS ONE*, *6*(1), e14553. https://doi.org/10.1371/journal.pone.0014553

Gleason, C. A., & Juul, S. E. (2017). Developmental biology of the heart. In *Avery's diseases of the newborn e-book* (3rd ed., pp. 724-740). Elsevier Health Sciences. https://doi.org/10.1016/B978-0-323-40139-5.00050-4

Goetz, S. C., & Anderson, K. V. (2010). The primary cilium: a signalling centre during vertebrate development. *Nature Reviews Genetics*, *11*(5), 331-344. https://doi.org/10.1038/nrg2774

Gokey, J. J., Ji, Y., Tay, H. G., Litts, B., & Amack, J. D. (2015). Kupffer's vesicle size threshold for robust left-right patterning of the zebrafish embryo. *Developmental Dynamics*, *245*(1), 22-33. https://doi.org/10.1002/dvdy.24355

Grimes, D. T., Boswell, C. W., Morante, N. F., Henkelman, R. M., Burdine, R. D., & Ciruna, B. (2016). Zebrafish models of idiopathic scoliosis link cerebrospinal fluid flow defects to spine curvature. *Science*, *352*(6291), 1341-1344. https://doi.org/10.1126/science.aaf6419

Grimes, D. T., & Burdine, R. D. (2017). Left–right patterning: breaking symmetry to asymmetric morphogenesis. *Trends in Genetics*, *33*(9), 616-628. https://doi.org/10.1016/j.tig.2017.06.004

Guichard, C., Harricane, M., Lafitte, J., Godard, P., Zaegel, M., Tack, V., & Bouvagnet, P. (2001). Axonemal dynein intermediate-chain gene (dnai1) mutations result in situs inversus and primary ciliary dyskinesia (kartagener syndrome). *The American Journal of Human Genetics*, *68*(4), 1030-1035. https://doi.org/10.1086/319511

Hao, L., & Scholey, J. M. (2009). Intraflagellar transport at a glance. *Journal of Cell Science*, *122*(7), 889-892. https://doi.org/10.1242/jcs.023861

Harrison, M. J., Shapiro, A. J., & Kennedy, M. P. (2016). Congenital heart disease and primary ciliary dyskinesia. *Paediatric Respiratory Reviews*, *18*, 25-32. https://doi.org/10.1016/j.prrv.2015.09.003

Horani, A., Druley, T., Zariwala, M., Patel, A., Levinson, B., Van Arendonk, L., & Ferkol, T. (2012). Whole-exome capture and sequencing identifies heatr2 mutation as a cause of primary ciliary dyskinesia. *The American Journal of Human Genetics*, *91*(4), 685-693. https://doi.org/10.1016/j.ajhg.2012.08.022

Horani, A., Ferkol, T. W., Shoseyov, D., Wasserman, M. G., Oren, Y. S., Kerem, B., & Kerem, E. (2013). Lrrc6 mutation causes primary ciliary dyskinesia with dynein arm defects. *PLoS ONE*, *8*(3), e59436. https://doi.org/10.1371/journal.pone.0059436

Hou, Y., Qin, H., Follit, J. A., Pazour, G. J., Rosenbaum, J. L., & Witman, G. B. (2007). Functional analysis of an individual ift protein: ift46 is required for transport of outer dynein arms into flagella. *The Journal of Cell Biology*, *176*(5), 653-665. https://doi.org/10.1083/jcb.200608041

Howe, K., Clark, M. D., Torroja, C. F., Torrance, J., Berthelot, C., Muffato, M., & Stemple, D. L. (2013). The zebrafish reference genome sequence and its relationship to the human genome. *Nature*, *496*(7746), 498-503. https://doi.org/10.1038/nature12111

Ibañez-Tallon, I., Pagenstecher, A., Fliegauf, M., Olbrich, H., Kispert, A., Ketelsen, U., & Omran, H. (2004). Dysfunction of axonemal dynein heavy chain mdnah5 inhibits ependymal flow and reveals a novel mechanism for hydrocephalus formation. *Human Molecular Genetics*, *13*(18), 2133-2141. https://doi.org/10.1093/hmg/ddh219

Jaakola, L., Pirttilä, A. M., Vuosku, J., & Hohtola, A. (2004). Method based on electrophoresis and gel extraction for obtaining genomic dna-free cdna without dnase treatment. *BioTechniques*, *37*(5), 744-748. https://doi.org/10.2144/04375bm06

Jain, V., Jain, J., & Gupta, O. (2011). A rare case of situs inversus with dextrocardia, lutembacher syndrome, and pericardial effusion. *Heart Views*, *12*(3), 107. https://doi.org/10.4103/1995-705x.95066

Jinek, M., Chylinski, K., Fonfara, I., Hauer, M., Doudna, J. A., & Charpentier, E. (2012). A programmable dual-rna-guided dna endonuclease in adaptive bacterial immunity. *Science*, *337*(6096), 816-821. https://doi.org/10.1126/science.1225829

Kamiya, R. (1988). Mutations at twelve independent loci result in absence of outer dynein arms in chylamydomonas reinhardtii. *The Journal of Cell Biology*, *107*(6), 2253-2258. https://doi.org/10.1083/jcb.107.6.2253

Kawakami, Y., Raya, Á., Raya, R. M., Rodríguez-Esteban, C., & Belmonte, J. C. (2005). Retinoic acid signalling links left–right asymmetric patterning and bilaterally symmetric somitogenesis in the zebrafish embryo. *Nature*, *435*(7039), 165-171. https://doi.org/10.1038/nature03512

Keeling, J., Tsiokas, L., & Maskey, D. (2016). Cellular mechanisms of ciliary length control. *Cells*, *5*(1), 6. https://doi.org/10.3390/cells5010006

Khodiyar, V. K., Howe, D., Talmud, P. J., Breckenridge, R., & Lovering, R. C. (2013). From zebrafish heart jogging genes to mouse and human orthologs: using gene ontology to investigate mammalian heart development. *F1000Research*, *2*, 242. https://doi.org/10.12688/f1000research.2-242.v1

Knowles, M. R., Zariwala, M., & Leigh, M. (2016). Primary ciliary dyskinesia. *Clinics in Chest Medicine*, *37*(3), 449-461. https://doi.org/10.1016/j.ccm.2016.04.008

Kobe, B. (2001). The leucine-rich repeat as a protein recognition motif. *Current Opinion in Structural Biology*, *11*(6), 725-732. https://doi.org/10.1016/s0959-440x(01)00266-4

Kramer-Zucker, A. G. (2005). Cilia-driven fluid flow in the zebrafish pronephros, brain and kupffer's vesicle is required for normal organogenesis. *Development*, *132*(8), 1907-1921. https://doi.org/10.1242/dev.01772

Leigh, M. W., Pittman, J. E., Carson, J. L., Ferkol, T. W., Dell, S. D., Davis, S. D., & Zariwala, M. A. (2009). Clinical and genetic aspects of primary ciliary dyskinesia/kartagener syndrome. *Genetics in Medicine*, *11*(7), 473-487. https://doi.org/10.1097/gim.0b013e3181a53562

Lindemann, C. B., & Lesich, K. A. (2010). Flagellar and ciliary beating: the proven and the possible. *Journal of Cell Science*, *123*(4), 519-528. https://doi.org/10.1242/jcs.051326

Liu, D., Wang, Z., Xiao, A., Zhang, Y., Li, W., Zu, Y., & Zhang, B. (2014). Efficient gene targeting in zebrafish mediated by a zebrafish-codon-optimized cas9 and evaluation of off-targeting effect. *Journal of Genetics and Genomics*, *41*(1), 43-46. https://doi.org/10.1016/j.jgg.2013.11.004

Lobo, L. J., Zariwala, M. A., & Noone, P. G. (2014). Primary ciliary dyskinesia. *QJM*, *107*(9), 691-699. https://doi.org/10.1093/qjmed/hcu063

Loges, N. T., Olbrich, H., Fenske, L., Mussaffi, H., Horvath, J., Fliegauf, M., & Omran, H. (2008). Dnai2 Mutations Cause primary ciliary dyskinesia with defects in the outer dynein arm. *The American Journal of Human Genetics*, *83*(5), 547-558. https://doi.org/10.1016/j.ajhg.2008.10.001

Long, S., Ahmad, N., & Rebagliati, M. (2003). The zebrafish nodal-related gene southpaw is required for visceral and diencephalic left-right asymmetry. *Development*, *130*(11), 2303-2316. https://doi.org/10.1242/dev.00436

Louvi, A., & Grove, E. (2011). Cilia in the cns: the quiet organelle claims center stage. *Neuron*, *69*(6), 1046-1060. https://doi.org/10.1016/j.neuron.2011.03.002

Malicki, J., Avanesov, A., Li, J., Yuan, S., & Sun, Z. (2011). Analysis of cilia structure and function in zebrafish. *Methods in Cell Biology*, *101*, 39-74. https://doi.org/10.1016/b978-0-12-387036-0.00003-7

Mall, M. A. (2008). Role of cilia, mucus, and airway surface liquid in mucociliary dysfunction: lessons from mouse models. *Journal of Aerosol Medicine*, *0*(0), 080116123756336-12. https://doi.org/10.1089/jam.2007.0659

Mangos, S., Lam, P. Y., Zhao, A., Liu, Y., Mudumana, S., Vasilyev, A., & Drummond, I. A. (2010). The adpkd genes pkd1a/b and pkd2 regulate extracellular matrix formation. *Development*, *137*(11), e1107-e1107. https://doi.org/10.1242/dev.053595

Marshall, W. F., Qin, H., Brenni, M. R., & Rosenbaum, J. L. (2005). Flagellar length control system: testing a simple model based on intraflagellar transport and turnover. *Molecular Biology of the Cell*, *16*(1), 270-278. https://doi.org/10.1091/mbc.e04-07-0586

Marshall, W. F., & Rosenbaum, J. L. (2001). Intraflagellar transport balances continuous turnover of outer doublet microtubules. *The Journal of Cell Biology*, *155*(3), 405-414. https://doi.org/10.1083/jcb.200106141

Matsui, T., & Bessho, Y. (2012). Left–right asymmetry in zebrafish. *Cellular and Molecular Life Sciences*, *69*(18), 3069-3077. https://doi.org/10.1007/s00018-012-0985-6

Meeker, N. D., Hutchinson, S. A., Ho, L., & Trede, N. S. (2007). Method for isolation of pcr-ready genomic dna from zebrafish tissues. *BioTechniques*, *43*(5), 610-614. https://doi.org/10.2144/000112619

Mitchison, H. M., & Valente, E. M. (2016). Motile and non-motile cilia in human pathology: from function to phenotypes. *The Journal of Pathology*, *241*(2), 294-309. https://doi.org/10.1002/path.4843

Mujo, T., Finnegan, T., Joshi, J., Wilcoxen, K. A., & Reed, J. C. (2015). Situs ambiguous, levocardia, right sided stomach, obstructing duodenal web, and intestinal nonrotation: a case report. *Journal of Radiology Case Reports*, *9*(2). https://doi.org/10.3941/jrcr.v9i2.2358

Murray, K. F., Larson, A. M., Masyuk, T. V., Masyuk, A. I., & LaRusso, N. F. (2010). Cholangiocyte cilia and basal bodies. In *Fibrocystic diseases of the liver* (pp. 45-70). Springer Science & Business Media. https://doi-org.proxy.bib.uottawa.ca/10.1007/978-1-60327-524-8_3

Männer, J. (2009). The anatomy of cardiac looping: A step towards the understanding of the morphogenesis of several forms of congenital cardiac malformations. *Clinical Anatomy*, *22*(1), 21-35. https://doi.org/10.1002/ca.20652

Nachury, M. V., Seeley, E. S., & Jin, H. (2010). Trafficking to the ciliary membrane: how to get across the periciliary diffusion barrier? *Annual Review of Cell and Developmental Biology*, *26*(1), 59-87. https://doi.org/10.1146/annurev.cellbio.042308.113337

Nauli, S. M., Kawanabe, Y., Kaminski, J. J., Pearce, W. J., Ingber, D. E., & Zhou, J. (2008). Endothelial cilia are fluid shear sensors that regulate calcium signaling and nitric oxide production through polycystin-1. *Circulation*, *117*(9), 1161-1171. https://doi.org/10.1161/circulationaha.107.710111

Nemtsas, P., Wettwer, E., Christ, T., Weidinger, G., & Ravens, U. (2010). Adult zebrafish heart as a model for human heart? An electrophysiological study. *Journal of Molecular and Cellular Cardiology*, *48*(1), 161-171. https://doi.org/10.1016/j.yjmcc.2009.08.034

New England Biolabs. (2014). Crispr/cas9 and targeted genome editing: a new era in molecular biology. *NEB expressions*, (1), 3-5.

Nicastro, D. (2009). Cryo-electron microscope tomography to study axonemal organization. *Methods in Cell Biology*, *91*, 1-39. https://doi.org/10.1016/s0091-679x(08)91001-3

Omran, H., Kobayashi, D., Olbrich, H., Tsukahara, T., Loges, N. T., Hagiwara, H., & Takeda, H. (2008). Ktu/pf13 is required for cytoplasmic pre-assembly of axonemal dyneins. *Nature*, *456*(7222), 611-616. https://doi.org/10.1038/nature07471

Onoufriadis, A., Paff, T., Antony, D., Shoemark, A., Micha, D., Kuyt, B., & Mitchison, H. (2013). Splice-site mutations in the axonemal outer dynein arm docking complex gene ccdc114 cause primary ciliary dyskinesia. *The American Journal of Human Genetics*, *92*(1), 88-98. https://doi.org/10.1016/j.ajhg.2012.11.002

Paladini, D., & Volpe, P. (2007). *Ultrasound of congenital fetal anomalies: differential diagnosis and prognostic indicators*. CRC Press.

Pan, J. (2008). Cilia and ciliopathies: From chlamydomonas and beyond. *Science in China Series C: Life Sciences*, *51*(6), 479-486. https://doi.org/10.1007/s11427-008-0071-3

Pennarun, G., Escudier, E., Chapelin, C., Bridoux, A., Cacheux, V., Roger, G., & Duriez, B. (1999). Loss-of-function mutations in a human gene related to chlamydomonas reinhardtii dynein ic78 result in primary ciliary dyskinesia. *The American Journal of Human Genetics*, *65*(6), 1508-1519. https://doi.org/10.1086/302683

Pennekamp, P., Menchen, T., Dworniczak, B., & Hamada, H. (2015). Situs inversus and ciliary abnormalities: 20 years later, what is the connection? *Cilia*, *4*(1). https://doi.org/10.1186/s13630-014-0010-9

Pfister, K. K. (2015). Distinct functional roles of cytoplasmic dynein defined by the intermediate chain isoforms. *Experimental Cell Research*, *334*(1), 54-60. https://doi.org/10.1016/j.yexcr.2014.12.013

Pigino, G., Geimer, S., Lanzavecchia, S., Paccagnini, E., Cantele, F., Diener, D. R., & Lupetti, P. (2009). Electron-tomographic analysis of intraflagellar transport particle trains in situ. *The Journal of Cell Biology*, *187*(1), 135-148. https://doi.org/10.1083/jcb.200905103

Porter, M. E. (1996). Axonemal dyneins: assembly, organization, and regulation. *Current Opinion in Cell Biology*, *8*(1), 10-17. https://doi.org/10.1016/s0955-0674(96)80042-1

Praetorius, H., & Spring, K. (2001). Bending the mdck cell primary cilium increases intracellular calcium. *Journal of Membrane Biology*, *184*(1), 71-79. https://doi.org/10.1007/s00232-001-0075-4

Ran, F., Hsu, P., Lin, C., Gootenberg, J., Konermann, S., Trevino, A., & Zhang, F. (2013). Double nicking by rna-guided crispr cas9 for enhanced genome editing specificity. *Cell*, *155*(2), 479-480. https://doi.org/10.1016/j.cell.2013.09.040

Reiter, J. F., & Leroux, M. R. (2017). Genes and molecular pathways underpinning ciliopathies. *Nature Reviews Molecular Cell Biology*, *18*(9), 533-547. https://doi.org/10.1038/nrm.2017.60

Richter, C., Chang, J. T., & Fineran, P. C. (2012). Function and regulation of clustered regularly interspaced short palindromic repeats (crispr) / crispr associated (cas) systems. *Viruses*, *4*(10), 2291-2311. https://doi.org/10.3390/v4102291

Roberts, A. J., Kon, T., Knight, P. J., Sutoh, K., & Burgess, S. A. (2013). Functions and mechanics of dynein motor proteins. *Nature Reviews Molecular Cell Biology*, *14*(11), 713-726. https://doi.org/10.1038/nrm3667

Sarmah, B., Winfrey, V. P., Olson, G. E., Appel, B., & Wente, S. R. (2007). A role for the inositol kinase ipk1 in ciliary beating and length maintenance. *Proceedings of the National Academy of Sciences*, *104*(50), 19843-19848. https://doi.org/10.1073/pnas.0706934104

Sawamoto, K. (2006). New neurons follow the flow of cerebrospinal fluid in the adult brain. *Science*, *311*(5761), 629-632. https://doi.org/10.1126/science.1119133

Schmidts, M., Freshour, J., Loges, N., Dritsoula, A., Antony, D., Hirst, R., & Mitchison, H. (2012). Mutations in the dynein assembly factor pf22 (dnaaf3) cause primary ciliary dyskinesia with absent dynein arms. *Cilia*, *1*(S1). https://doi.org/10.1186/2046-2530-1-s1-p101

Schneider, I., Houston, D. W., Rebagliati, M. R., & Slusarski, D. C. (2007). Calcium fluxes in dorsal forerunner cells antagonize -catenin and alter left-right patterning. *Development*, *135*(1), 75-84. https://doi.org/10.1242/dev.004713

Scholey, J. M. (2008). Intraflagellar transport motors in cilia: moving along the cell's antenna. *The Journal of Cell Biology*, *180*(1), 23-29. https://doi.org/10.1083/jcb.200709133

Shah, A. S., Ben-Shahar, Y., Moninger, T. O., Kline, J. N., & Welsh, M. J. (2009). Motile cilia of human airway epithelia are chemosensory. *Science*, *325*(5944), 1131-1134. https://doi.org/10.1126/science.1173869

Shen, M. M. (2007). Nodal signaling: developmental roles and regulation. *Development*, *134*(6), 1023-1034. https://doi.org/10.1242/dev.000166

Smith, K. A., Noël, E., Thurlings, I., Rehmann, H., Chocron, S., & Bakkers, J. (2011). Bmp and nodal independently regulate lefty1 expression to maintain unilateral nodal activity during left-right axis specification in zebrafish. *PLoS Genetics*, *7*(9), e1002289. https://doi.org/10.1371/journal.pgen.1002289

Song, Z., Zhang, X., Jia, S., Yelick, P. C., & Zhao, C. (2016). Zebrafish as a model for human ciliopathies. *Journal of Genetics and Genomics*, *43*(3), 107-120. https://doi.org/10.1016/j.jgg.2016.02.001

Sorokin, S. (1962). Centrioles and the formation of rudimentary cilia by fibroblasts and smooth muscle cells. *The Journal of Cell Biology*, *15*(2), 363-377. https://doi.org/10.1083/jcb.15.2.363

Sorokin, S. P. (1968). Reconstructions of centriole formation and ciliogenesis in mammalian lungs. *Journal of Cell Science*, *3*, 207-230. http://jcs.biologists.org/

Sternberg, S. H., Redding, S., Jinek, M., Greene, E. C., & Doudna, J. A. (2014). Dna interrogation by the crispr rna-guided endonuclease cas9. *Nature*, *507*(7490), 62-67. https://doi.org/10.1038/nature13011

Swarts, D. C., Mosterd, C., Van Passel, M. W., & Brouns, S. J. (2012). Crispr interference directs strand specific spacer acquisition. *PLoS ONE*, *7*(4), e35888. https://doi.org/10.1371/journal.pone.0035888

Taschner, M., Mourão, A., Awasthi, M., Basquin, J., & Lorentzen, E. (2017). Structural basis of outer dynein arm intraflagellar transport by the transport adaptor protein oda16 and the intraflagellar transport protein ift46. *Journal of Biological Chemistry*, *292*(18), 7462-7473. https://doi.org/10.1074/jbc.m117.780155

Thisse, C., & Thisse, B. (2007). High-resolution in situ hybridization to whole-mount zebrafish embryos. *Nature Protocols*, *3*(1), 59-69. https://doi.org/10.1038/nprot.2007.514

Tran, D. Q., Andersson, J., Wang, R., Ramsey, H., Unutmaz, D., & Shevach, E. M. (2009). Garp (lrrc32) is essential for the surface expression of latent tgf- on platelets and activated foxp3+ regulatory t cells. *Proceedings of the National Academy of Sciences*, *106*(32), 13445-13450. https://doi.org/10.1073/pnas.0901944106

Van Rooijen, E., Giles, R. H., Voest, E. E., Van Rooijen, C., Schulte-Merker, S., & Van Eeden, F. J. (2008). LRRC50, a conserved ciliary protein implicated in polycystic kidney disease. *Journal of the American Society of Nephrology*, *19*(6), 1128-1138. https://doi.org/10.1681/asn.2007080917

Veland, I. R., Awan, A., Pedersen, L. B., Yoder, B. K., & Christensen, S. T. (2009). Primary cilia and signaling pathways in mammalian development, health and disease. *Nephron Physiology*, *111*(3), p39-p53. https://doi.org/10.1159/000208212

Voss, F. K., Ullrich, F., Munch, J., Lazarow, K., Lutter, D., Mah, N., & Jentsch, T. J. (2014). Identification of lrrc8 heteromers as an essential component of the volume-regulated anion channel vrac. *Science*, *344*(6184), 634-638. https://doi.org/10.1126/science.1252826

Wang, G., Yost, H. J., & Amack, J. D. (2013). Analysis of gene function and visualization of cilia-generated fluid flow in kupffer's vesicle. *Journal of Visualized Experiments*, (73). https://doi.org/10.3791/50038

Wanner, A., Salathé, M., & O'Riordan, T. G. (1996). Mucociliary clearance in the airways. *American Journal of Respiratory and Critical Care Medicine*, *154*(6), 1868-1902. https://doi.org/10.1164/ajrccm.154.6.8970383

Warga, R. M., & Stainier, D. Y. (2002). The guts of endoderm formation. *Results and Problems in Cell Differentiation*, *40*, 28-47. https://doi.org/10.1007/978-3-540-46041-1_3

Wickstead, B., & Gull, K. (2007). Dyneins across eukaryotes: a comparative genomic analysis. *Traffic*, *8*(12), 1708-1721. https://doi.org/10.1111/j.1600-0854.2007.00646.x

Yoshiba, S., & Hamada, H. (2014). Roles of cilia, fluid flow, and ca2+ signaling in breaking of left–right symmetry. *Trends in Genetics*, *30*(1), 10-17. https://doi.org/10.1016/j.tig.2013.09.001

Zariwala, M. A., Knowles, M. R., & Leigh, M. W. (2015). Primary ciliary dyskinesia. In *GeneReviews®*.

Zhu, X., Xu, Y., Yu, S., Lu, L., Ding, M., Cheng, J., & Tian, Y. (2014). An efficient genotyping method for genome-modified animals and human cells generated with crispr/cas9 system. *Scientific Reports*, *4*(1). https://doi.org/10.1038/srep06420